International Journal of Solids and Structures 284 (2023) 112501

Contents lists available at ScienceDirect

International Journal of Solids and Structures

journal homepage: www.elsevier.com/locate/ijsolstr

Investigation of the compressive properties of three-dimensional Voronoi reticula

Ivan Colamartino [a,*], Marco Anghileri [b], Marco Boniardi [a]

[a] Dipartimento di Meccanica, Politecnico di Milano, Via La Masa 1, Milan, 20156, Italy
[b] Dipartimento di Scienze e Tecnologie Aerospaziali, Politecnico di Milano, Via La Masa 34, Milan, 20156, Italy

ARTICLE INFO

Dataset link: lattice300

Keywords:
Voronoi reticula
Stochastic foams
Cellular materials
Strut-based lattices

ABSTRACT

With the rise of additive manufacturing technologies, artificial production of stochastic cellular materials is becoming increasingly more feasible and convenient, exposing the need of accurate models able to predict their mechanical properties. However, the construction of generalized predictive models for stochastic structures is non-trivial: on the one hand, this is due to the several potential base materials, and on the other it is because of the difficulty in implementing geometrically accurate numerical models. In light of these considerations, the present work presents a systematic analysis of one the most known – and commonly used – stochastic cellular structure, the Voronoi three-dimensional lattices; the aim is providing simple empirical relations between the main properties of a generic base material and the compressive properties of the related additively manufactured stochastic Voronoi reticulum as a function of its geometry. The investigation provides novel insights on the mechanical properties of Voronoi reticula, highlighting superior efficiency with respect to their natural counterpart, the open-cell foams, and exposing unsuitability of classical equations for accurate prediction of their mechanical properties.

1. Introduction

Cellular materials have always risen interest in many fields of science and engineering. Traditionally found in nature (trabecular bones (Oftadeh et al., 2015), fungi (Nelson, 2021), honeycomb structures (Hales, 2001), etc.), natural cellular materials have evolved over millions of years targeting achievement of specific functions, such as providing strength and support, regulating temperature, and facilitating gas exchange. Aided by the rise of effective manufacturing technologies such as additive manufacturing and by the advancements in numerical modelling methodologies, scientists have analysed and synthetically reproduced such materials, reporting high specific performances (Gibson, 2003) such as strength, stiffness, impact resistance, thermal and acoustic properties (Kumar et al., 2009; Fiedler et al., 2009; Wang and Lu, 1999), and in general attractive multi-functional and versatile behaviour (Rahman et al., 2022). Today, some of the several applications are lightweight components for aerospace and automotive engineering (Bornengo et al., 2005; Hohe et al., 2012; Patten et al., 1998; Bisht et al., 2019), thermal/sound insulation (Ge and Zhai, 2018; Arcaro et al., 2016), bio-medical and tissue engineering (Limmahakhun et al., 2017; Wen et al., 2002), energy and impact absorption (Vesenjak et al., 2008; Linul et al., 2014).

Cellular structures may be classified in multiple manners. Amongst those, one of the most widely accepted is the spatial arrangement of the microstructure, non-stochastic or stochastic: the former, characterized by regular topology consisting in periodic repetition of a unit cell, are commonly orthotropic (Zhang and Ashby, 1992; Papka and Kyriakides, 1998) with peculiar and often architected mechanical properties different as a function of the loading direction (Maskery et al., 2017); the latter, conversely, are characterized by randomatic or quasi-randomatic geometries and consequent irregular patterns, typically reporting isotropy when sufficiently large to cancel out boundary effects and when no directionality is caused by the production process (Huber and Gibson, 1988). Another significant classification is related to the topology of the cells, which may be closed (sheet-based) or open (strut-based); the first category is commonly characterized by higher densities and stiffness, while the second by lower densities and higher flexibility (Chan and Nakamura, 1969; Azzi et al., 2004; Andrews et al., 1999). For many applications isotropy is generally desirable: for instance when loading condition could be not known a priori and/or mechanical properties need to be valid in spite of the loading direction. In these cases, stochastic cellular structures may be looked at.

* Corresponding author.
E-mail address: ivan.colamartino@polimi.it (I. Colamartino).

https://doi.org/10.1016/j.ijsolstr.2023.112501
Received 28 June 2023; Received in revised form 21 August 2023; Accepted 30 September 2023
Available online 7 October 2023

Several studies on stochastic foams were published over the last decades. Studies primarily focused on the experimental analysis of open and closed-cell foams, which are found in nature (trabecular bones) or can be generated artificially (polymeric, metallic foams): the analyses provided wide knowledge on their thermal, acoustic and mechanical behaviour (Davies and Zhen, 1983; Yu and Banhart, 1997), later extended to strain-rate dependency for better understanding of their energy absorption capabilities (Ouellet et al., 2006; Dannemann and Lankford, 2000). Parallelly, two main strategies were considered and studied for numerical reproduction of the foam behaviour. The first, based on the studies of Lord Kelvin in the second half of the XIXth century, exploits the so-called *Kelvin cell*, or tetrakaidecahedron, a convex polyhedron that showed for decades to be the best solution for optimal approximations of real foams (Sullivan et al., 2008; De Giorgi et al., 2010) and still remains a valid tool for many applications (Sabet et al., 2023; Kirpluks et al., 2023) thanks to its periodic nature allowing relatively easy modelling buildups. The second strategy, more recent and driven by the will to better describe the stochastic nature of the foams and analyse potentially better modelling solutions (Jang et al., 2010), directly implements the randomness of the foams by reconstructing the geometry via Non-Destructive Inspections (NDI) such as Computerized Tomography (CT) scans, by approximating it via tessellation procedures, and often by a combination of the two methods (Lautensack and Sych, 2006; Schladitz et al., 2012; Wejrzanowski et al., 2013); in the last decade, this second strategy has rapidly become the most used in scientific research, and allowed for accurate reconstruction and ultimately better understanding of the physics of stochastic foams (Gaitanaros and Kyriakides, 2015; Stiapis et al., 2019; Chen et al., 2020; Wang et al., 2021; Al-Osman et al., 2023).

The aforementioned studies focused on the analysis, reproduction or numerical modelling of natural and artificial foams, while as of today little research has been provided for the modelling of three-dimensional strut-based Voronoi lattices; in fact, even if the second have been historically used for the approximation of the first via the procedures described above, the two geometries have fundamental topological differences that is here hypothesized could potentially affect their mechanical behaviour: in particular, natural foams are characterized by smooth and filleted geometry, while lattices are more similar to theoretical structures such as truss-based or thin-walled engineering constructions. The need to dive into comprehensive numerical analyses of ideal Voronoi reticula to confirm or confute such hypothesis has not emerged in the last two decades for the main reason that such idealization has been used for approximating natural geometries, and ideal lattices were simply not of interest as not found in nature. With modern manufacturing technologies however, it is today possible to target the most efficient structural configurations at the smallest scales, and the need of reliable predictive models for ideal stochastic structures is becoming increasingly more evident.

First notable publications on the subject have been authored between 2015 and 2018, when G. Maliaris et al. studied experimentally and numerically the response of Voronoi lattices exploiting investment casting techniques for A1100 aluminium and AISI304 steel (Maliaris et al., 2016) and SLA (Stereolithography) additive technologies for the Asiga PlasGRAY photopolymer (Maliaris and Sarafis, 2017); to the authors' knowledge, these studies remain today the only analyses based on solid-meshed numerical models, even if it was later chosen to abandon such technique in favour of homogenization solutions (Maliaris et al., 2018). Later, comparison with regular topologies was provided for the mechanical properties of additively manufactured Al6101, Ti6Al4V and AlSi10Mg lattices (Mueller et al., 2019; Raghavendra et al., 2021; Shinde et al., 2022), while thermal behaviour of Ti6Al4V specimens was analysed in another notable study (Zhang et al., 2021). More recently, effects of irregularities in PA12 samples were investigated (Okubo et al., 2023). Essentially, all these studies have treated either the evaluation of the behaviour of a single material as a function of the geometrical parameters or the analysis in comparison with other topologies, or both. As a consequence, as of today literature still lacks a comprehensive predictive model for a sufficiently wide range of base materials not based on classical studies on open-cell foams, with geometrically accurate numerical models for evaluation of the Voronoi topology compared to such foams, and considering uncertainties over randomness and boundary effects.

Consequently, the present work focuses on three-dimensional stochastic Voronoi reticula and systematically studies its static compressive behaviour as a function of its main design and material parameters via high-quality solid-meshed numerical models, comparing the results with classical literature equations commonly used for the approximation of open-cell foams. The purpose is on the one hand to deepen the scientific knowledge on the behaviour of stochastic metamaterials, on the other to provide simple empirical models capable of predicting the structural parameters of Voronoi reticula for any base material, useful especially for design engineers active in the field of additive manufacturing. In contrast to most related literature, the present work systematically exploits solid meshes for the construction of generalized, predictive models for Voronoi lattices, as the authors believe that the beam theory is not applicable with suited accuracy for the scope of the work; such choice is justified later on in the document. It is ultimately shown, and proved within reasonable uncertainty by comparison to literature equations, that for three-dimensional strut-based Voronoi lattices a limited density variation with respect to their natural counterpart actually corresponds to notable variations of mechanical properties.

The document is structured as follows. The next section (Section 2) provides detailed description of the selected construction methodology for the Voronoi reticula, with considerations on contributions of boundary and stochasticity effects, geometrical and material parameters and FEM (Finite Element Method) modelling build-up. Then (Section 3), parametric analyses are reported, with focus on density, randomness and boundary effects and finally base material properties; subsequently, validation of the results through simple experimental tests on purposely-designed specimens is presented. Last, results are discussed and conclusions are drawn.

2. Material and methods

2.1. Perfect and non-perfect voronoi foams and literature approximations

Three-dimensional Voronoi reticula have traditionally been treated as open-cell foams, or *Voronoi foams*, and vice versa. Pioneering studies on such reticula have been published, amongst others, by L. J. Gibson and M. F. Ashby throughout the '90s and mid '00s (Gibson, 2003), providing simplified analytical equations for relative density, stiffness and collapse stress. Such authors grouped Voronoi foams based on their macroscopic compressive behaviour: elastomeric, elastic–plastic and brittle foams. The first show a large elastic phase typical of elastomers, the second are characterized by a plastic yielding collapse stress, the third present an oscillatory plateau caused by brittle crushing (Fig. 1).

Despite the evident differences, all the three show the typical compressive behaviour appreciated in most of cellular materials: initial elastic phase, collapse plateau and densification. Without diving quantitatively into the base material properties and peculiar collapse modes of each subcategory, an optimal behaviour in terms of uniformity and stability of the collapse phase can be identified in the elastic–plastic case: in fact, while elastomeric foams present hardening due to elastic buckling and brittle foams show highly unstable collapse, the plastic yielding seem to guarantee quasi-constant collapse stress. As such, the present work focuses on the analysis of Voronoi foams based on ductile plastics and metals, in other words foams for which predicted behaviour is elastic–plastic, theoretically described as a function of the

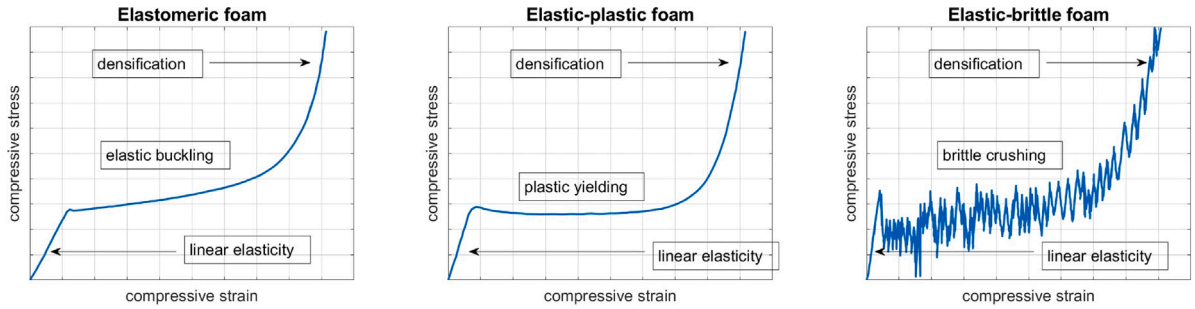

Fig. 1. Compressive behaviour of stochastic foams.
Source: Plots are re-created from Gibson (2003).

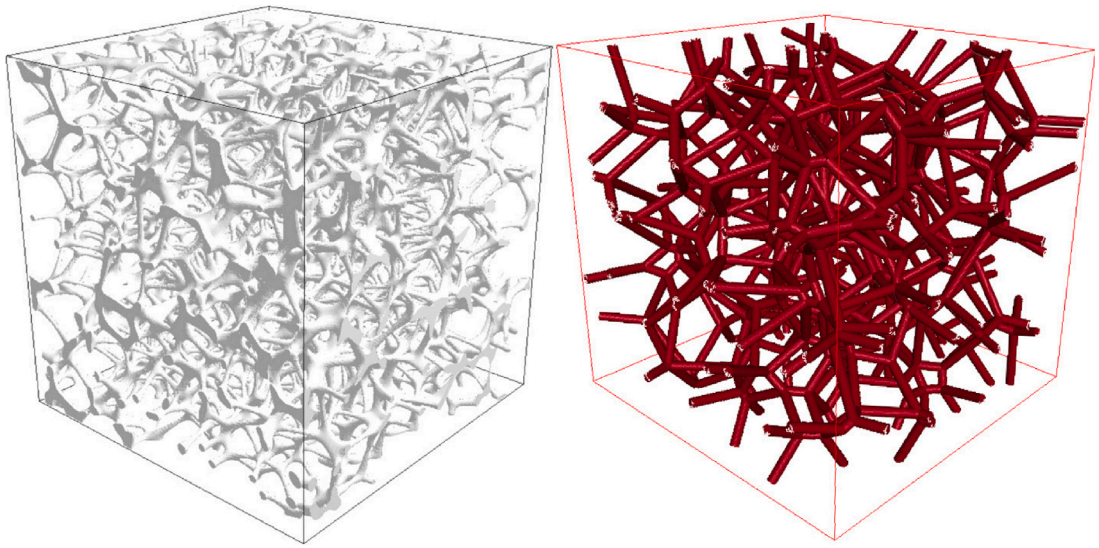

Fig. 2. Natural and artificial foams (left, August and Nestler (2020)) vs perfect Voronoi reticula (right).

relative density (RD) by the Gibson–Ashby relations provided below (Eqs. (1), (2), (3)):

$$RD\left(\frac{t}{l}\right) = C\left(\frac{t}{l}\right)^2 \tag{1}$$

$$E_{ret} = C\,(RD)^2\,E \approx (RD)^2\,E \tag{2}$$

$$Y_{ret} = C\,(RD)^{3/2}\,Y \approx 0.3\,(RD)^{3/2}\,Y \tag{3}$$

where t and l are strut thickness and length, E and Y elastic modulus and yield stress of the base material, RD, E_{ret} and Y_{ret} relative density, stiffness and collapse stress of the reticulum.

These equations, primarily based on experimental studies, can be referred to classical open-cell foams, characterized by three-dimensional fillets present at each node (Fig. 2), inevitably found in natural foams such as trabecular bones as nature strives to avoid stress-concentrating sharp edges; analogously, artificial polymeric and metallic foams follow the same physical laws. Natural foams and their artificial reproductions could then be identified as *geometrically imperfect* reticula characterized by composition of filleted beams, with substantial differences from ideal stochastic reticula, free of any fillet and created by direct composition of three-dimensional beams, with highest proximity to an ideal reticulum, composition of one-dimensional rods. In that sense, the latter may be identified as *perfect* reticula, where such term is referred to the proximity to an ideal reticulum, the configuration of maximum structural efficiency. In another sense, they could be described as a subcategory – optimal in terms of specific properties – of natural foams.

2.2. Voronoi generation

The construction of a generic cellular reticulum is, in principle, fairly simple: it is a union of multiple elementary geometries such as prisms, cylinders, cones. However, when practically approached, the task requires to compute the boolean union of several base geometries to get to the finalized structure and the simplicity of such base geometries is not sufficient to make the problem less costly. Moreover, Voronoi reticula are stochastic geometries, based on the homonymous tessellation scheme computed over a generic set of sample points; as such, further difficulty in their three-dimensional modelling lies in the absence of periodicity, which prevents to exploit cell-repetition schemes.

With the ascent of additive manufacturing technologies and the so-called Generative Design and Design for Additive Manufacturing (DfAM), the problem of cellular geometries generation – valid not only for beam reticula but for any cellular shape – has been approached with the aid of implicit modelling (Nguyen et al., 2021), which allows to strongly reduce the computational cost when the geometry is made of several repetitions of elementary base geometries. Nonetheless, in the present work implicit modelling solutions were set aside, as, to the authors' knowledge, all implicit modelling softwares targeted at cellular structures' design are today commercial and rather expensive: first obvious consequence in the use of such softwares would be difficult reproduction of the study results, or at least its dependency on those softwares themselves; second one would be a partial control over the geometry creation, fundamental to pursue a systematic analysis. Consequently, it was decided to carry out the design and modelling

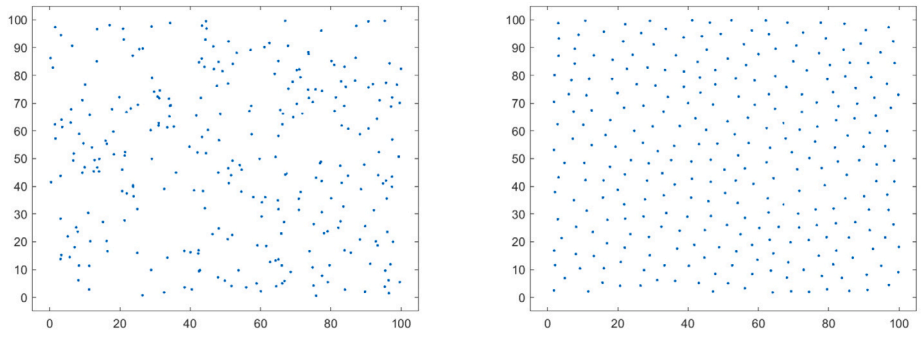

(a) Random samples (b) Quasi-random samples

Fig. 3. Poisson disk sampling in two dimensions: on the left, 285 random samples; on the right, 285 samples obtained through the Poisson disk algorithm with threshold set to 5 units.

phase only through open-source softwares. Voronoi reticula have been generated starting from random three-dimensional point clouds, subsequently tessellated under the Voronoi scheme and bounded by cuboid shapes. The generation mainly relies on Gmsh (Geuzaine and Remacle, 2009) and in particular its Python API (Application Program Interface) for optimal control. Concurrently to the geometry generation, Gmsh is exploited to compute high-quality tetrahedral mesh for subsequent FEM analyses.

2.2.1. Point cloud generation

The point cloud generation is a first key step for the structure design: in order to obtain a functional Voronoi structure, it is paramount to maintain stochasticity while guaranteeing uniform strut distribution. Such two requirements are however colliding, as pure random point distribution would be intrinsically non-uniform while uniform distributions are in fact regular distributions. The problem is here overcome by using quasi-random point clouds via the Poisson disk sampling algorithm. Such algorithm, based on the work of Siméon Denis Poisson (the Poisson distributions) and largely used especially in the field of computer graphics (Crow, 1977; Cook, 1986), is today general accepted as one of the best sampling patterns for a wide range of applications (Lagae and Dutré, 2008).

In practice, the Poisson disk algorithm here used is implemented through the classical *dart-throwing* scheme (Cook, 1986), indubitably the simplest between the ones available today in terms of implementation efforts and consisting in randomatic generation of points, with acceptance or rejection based on their distance to any other previously generated point: if the newly generated point is farther from any other previously accepted sample by more than a fixed threshold, the point is accepted. Clarifying pictures of two-dimensional subcase can be appreciated in Fig. 3, while effects on the reticulum structure is showed in the subsequent paragraph 2.2.2, Fig. 5. The scheme can be practically compared to the act of randomly throwing darts towards a circular target centred to the nearest accepted sample point, with the peculiar objective of striving to miss the target to gain a new successful throw; thus explained the aforementioned name.

Within the Poisson disk algorithm only two parameters are needed to completely define the sampling: one is the minimum distance between any points, the other is the termination condition. The first is actually the first structural parameter, and if set constant throughout the whole volume is a single scalar univocally determining the reticulum. The minimum distance is treated later on in the present section, paragraph 2.3. On the contrary, the termination condition is not geometry-related nor topology related; it is instead natural, inevitable heir of the sampling method. As such, in order to proceed with a systematic parametric analysis it is important to cancel out its effects, or – more likely – to push those effects to reasonably negligible values. As no direct correlation is evident with the structural behaviour, the problem is treated within the sampling phase, evaluating convergence in terms of finalized number of sampled points after termination. Sampling is performed on a $20 \times 20 \times 20$ mm cube,[1] with minimum distance set at 4 mm. The termination condition is implemented by limiting the maximum count of failed point generations per trial. Effects of increasing thresholds, 10^2 through 10^6, are reported in Fig. 4.

Results provided in Fig. 4 show the total dart throws and the finalized number of samples as a function of the termination condition: the first curve, drawn in logarithmic scale, shows linear increase of the computational costs as a function of the attempts threshold; the second curve shows that convergence is obtained with reasonable error when such threshold is set between 10^4 and 10^5, resulting in a number of samples between 120 and 130 for the analysed case. In light of these results, and in order to guarantee coherent data in terms of sampling, limit condition for all subsequent sample generations is set to 10^5, with an uncertainty error with respect to the converged value reported at 5%. It is assumed that such 5% uncertainty over the converged number of samples can be extended to any subsequent result reported at Section 3.

2.2.2. Reticulum generation and mesh

Once point cloud generation method is established, the tessellation is performed.

Briefly, the Voronoi diagram, output of such tessellation, is univocally defined for a given set of N points as the *nearest-neighbour map* for that set of points. The tessellation partitions the n-dimensional space in N regions (Voronoi cells), each related to one of the points (*nuclei*) such that any point inside each region is closer to its cell's nucleus than to any other nucleus. In two dimensions such tessellation translates in a set of N adjacent polygons, in three dimensions to a set of adjacent polyhedra. In both cases, if edges are extracted a stochastic reticulum is obtained.

The tessellation procedure can be carried out in multiple ways and several algorithms have been created for efficient computation.[2] In the present work tessellation is performed via the Python package scipy.spatial.Voronoi, from the Scipy ecosystem (Virtanen et al., 2020) calling the Qhull library (Barber et al., 1996). Voronoi edges are then extracted and implemented in Gmsh (Geuzaine and Remacle, 2009) through the Python API. Subsequently, still in the Gmsh environment, the obtained reticulum is cut via OpenCascade Gmsh routines to fit into

[1] Detailed information about bounding volumes for sampling and tessellation are provided in paragraph 2.3.

[2] It is here important to underline that as Voronoi tessellation is unique for a given set of points, there is no manoeuvring space to variate the geometrical parameters within tessellation phase, and as such the topology is univocally determined once the point cloud is generated. The second, and last, topology variation occurs in the choice of the strut properties, i.e. the cross sections.

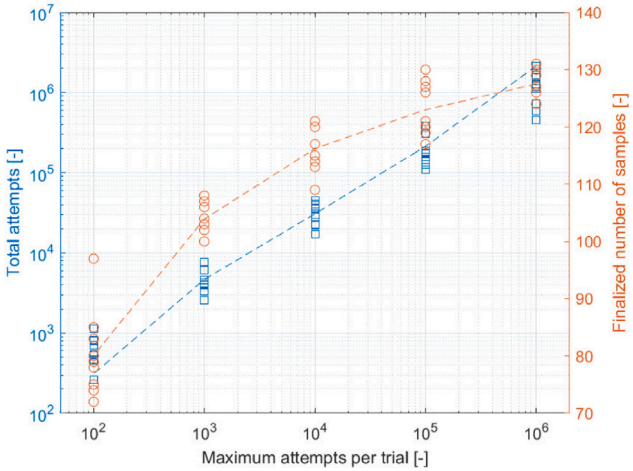

Fig. 4. Effect of Poisson disk sampling termination condition on the sample count. Semi-logarithmic scale is used for improved clarity.

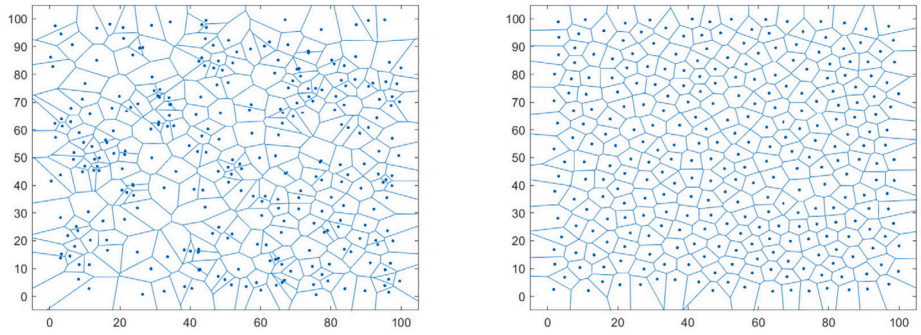

(a) Random samples (b) Quasi-random samples

Fig. 5. Voronoi tessellation in two-dimensions; point clouds are the same reported in Fig. 3.

a cuboid. Finalized geometry is obtained by creating cylinders for each Voronoi edges, and finally performing a boolean union of all the struts.

When the geometry is obtained, the Gmsh API is used for a last task, which is the tetrahedral meshing. Meshing is performed through the most robust from the available algorithms in Gmsh, the "Delaunay" algorithm (Geuzaine and Remacle, 2003; Frey and George, 2007; Si and TetGen, 2006). The choice of such solid meshing, which is known to increase considerably computational costs with respect to simpler beam meshes, is explained in paragraph 2.3, along with detailed overview of the meshing parameters.

Scheme of the computational framework for the Voronoi design is showed in Fig. 6.

2.3. Parameters' definition and selection

The present section is dedicated to the definition of the Voronoi structures and the parametrization which will determine the subsequent analyses' steps.

2.3.1. Voronoi geometric parameters

Voronoi reticula built as described in the previous paragraph are univocally defined by sampled points, bounding volume and strut cross-section properties. In order to proceed with the analyses, these three elements are here translated into two main parameters: Poisson minimum distance and strut diameter, respectively here named λ and D. The first may be called *characteristic length*, as univocally determining the reticulum: in a regular cellular geometry it would correspond to the cell size (Fig. 7).

In order to provide a unique variable to describe the reticulum topology, another parameter is then defined as follows:

$$\alpha = \frac{\lambda}{D} \tag{4}$$

Such parameter is not only a mere density indicator but assumes significant structural meaning, traceable to a *slenderness ratio*, providing qualitative indication of the reticulum stiffness. The parameter α is useful to explain the need of a tetrahedral mesh and define the range of interest.

In particular, if lengths of all the beams for a generic subcase are analysed, it is reported that the aforementioned slenderness ratio is far from being a representative parameter for every strut. In fact, by taking one subcase, in particular one iteration of "L4D.8" ($\lambda = 4$, $D = .8$ mm), it is shown (Fig. 8) that most of the struts present relative lengths (L/λ) around 0.2 and 0.8, being 20%–80% of the minimum distance 4 mm. It is worth noting that for a theoretical $\alpha = \lambda/D = 5$, local ratios reach values down to $\alpha_{local} = .2\alpha = 1$: translating in physical terms, a beam with equal length and diameter.

The present result, especially evident at high relative densities but valid for all slenderness ratios and peculiar of the Voronoi geometry, is fundamental to understand that the applicability of the beam theory for FEM analysis of Voronoi reticula could be rather problematic, and at best would require a model-dependent validation phase to assure the proper behaviour of each strut. Consequently, and being the present study focused on the construction of predictive numerical models targeted to parametric analyses, it was decided to proceed with a solid tetrahedral mesh, not prone to such problem.

In terms of range of interest, preliminary analyses reported values of $RD \sim .3$ for $\alpha \sim 2.5$, meaning a minimum sampling threshold 2.5 times

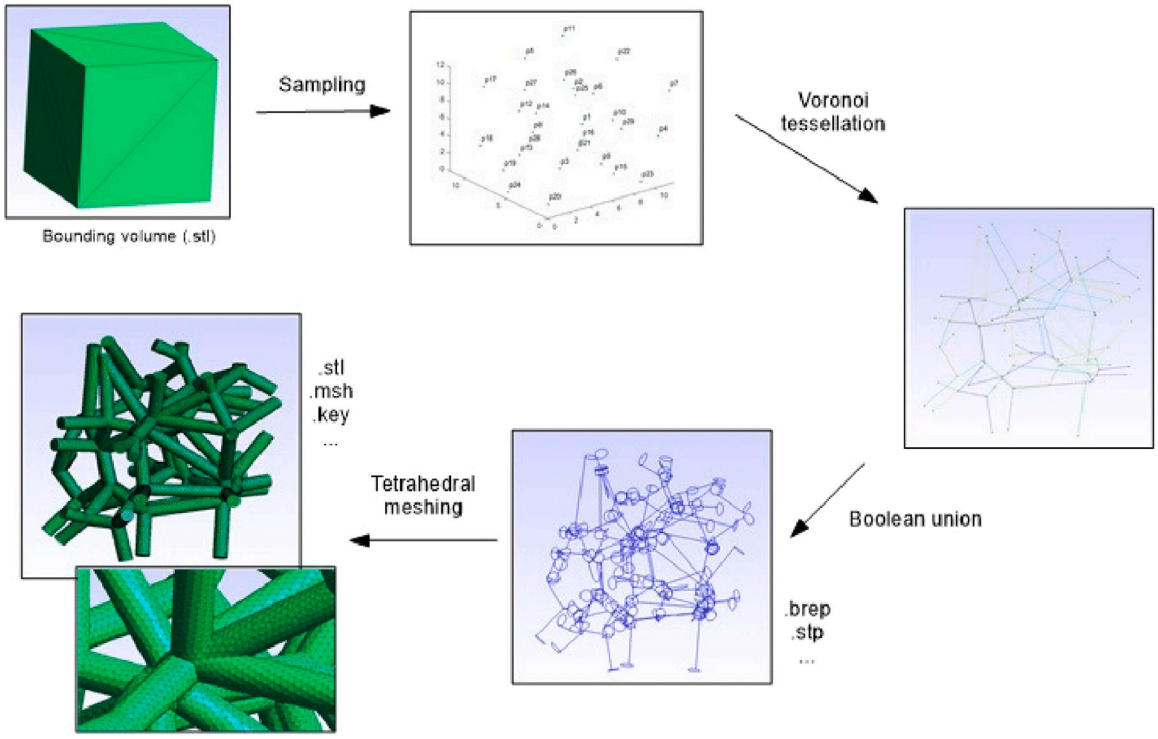

Fig. 6. Voronoi generation, computational framework.

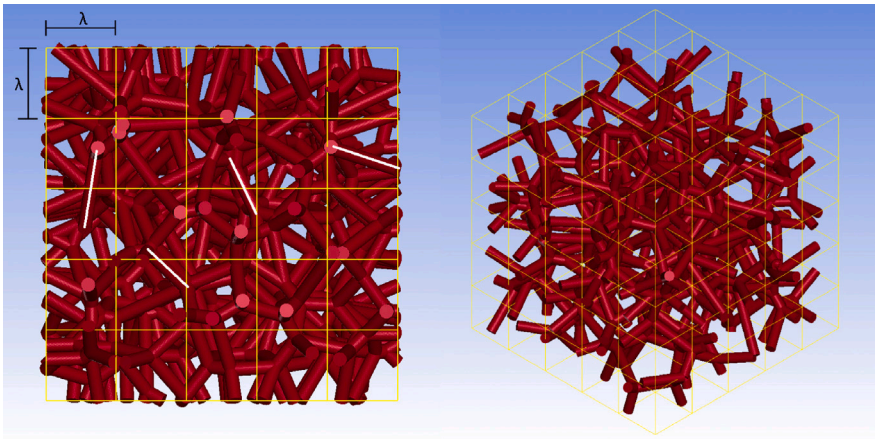

Fig. 7. Characteristic length λ, front and perspective view.

greater than the diameter: such value, conservatively beyond the limit both for literature common thresholds ($RD = .2$, Gibson (2003)) and for assuring advantages in practical applications where mass minimization is the primary objective, is taken in this study as the upper bound of relative density for compliance to a Voronoi reticulum.

Subsequently, significant variables would be the *characteristic dimensions*, which determine the cuboid dimensions in the three directions; such variables may be defined as N_x, N_y, N_z in terms of units of cells:

$$N_x = \frac{L_x}{\lambda} \tag{5}$$

$$N_y = \frac{L_y}{\lambda} \tag{6}$$

$$N_z = \frac{L_z}{\lambda} \tag{7}$$

where L_x, L_y, L_z are the dimensions of the cuboid in x, y, z. For a cubic shape: $N_x = N_y = N_z = N$. The parameter N is significant for guaranteeing homogeneous behaviour avoiding boundary effects: mechanical response of cellular solids is known to be sensitive to the number of resisting cells, with strong variation of the properties when such number is low. If conservative threshold for excluding this effects is often accepted at $N = 10$, for our purposes such value would lead to enormous models and consequent unfeasible computational costs: for this reason, for each of the analyses performed a preliminary cell sensitivity study is carried out to find the lowest possible characteristic dimension guaranteeing reasonably negligible boundary effects. It will be showed later on through the document that for all the analysed cases, $N = 5$ turned out to be an acceptable threshold. For what concerns the mesh sensitivity, analyses were acceptable for meshes where maximum tetrahedral dimension was $1/4_{th}$ of the diameter; nonetheless, conservative choice of $1/8_{th}$ was taken to safely neglect consequences of mesh sensitivity. A fixed diameter of 0.8 mm was chosen setting consequently 0.1 mm as mesh maximum dimension and leaving λ as only variable for all the analysed cases. Overview of the

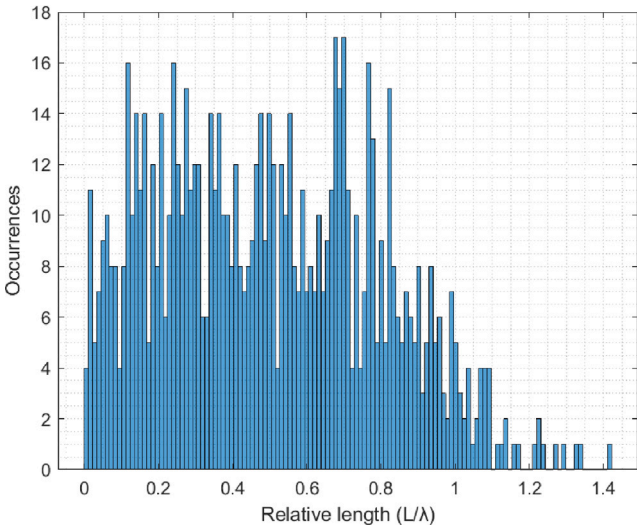

Fig. 8. Distribution of strut relative lengths for subcase "L4D.8".

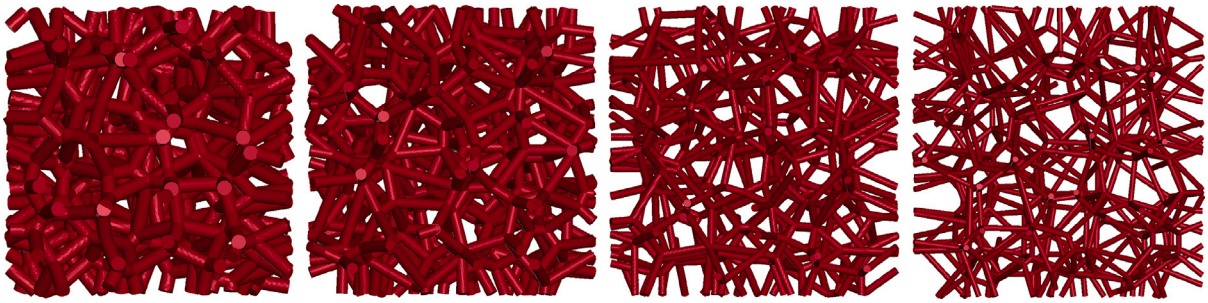

Fig. 9. FE models for geometries reported at Table 1 (left to right).

Table 1
FE models – mesh details.

N	λ [mm]	D [mm]	α [–]	RD [%]	avg. nodes [–]	avg. elements [–]
5	3	.8	3.75	15.4	160,558	576,437
5	4	.8	5	9.3	535,422	2,176,548
5	6	.8	7.5	4.3	796,239	3,211,932
5	8	.8	10	2.3	1,133,336	4,560,546

mesh parameters for subcases with $N = 5$ is provided in Table 1, while front views of four models at different values of α are shown in Fig. 9.

2.3.2. Material parameters

In terms of material properties, the purpose of the study is to find generalized criteria for the prediction of stiffness (E_{rel}) and collapse stress (Y_{rel}) of Voronoi stochastic reticula for a generic material; as such, selection of interesting materials is bound to the practical usefulness and manufacturability of the structure itself. Traditionally, the most used manufacturing technology for production of stochastic open-cell foams has been the foaming process, effective in producing components with extremely low relative densities down to 1%–2%, both for plastics such as polyurethane or polypropylene, or metals as aluminium; however, these processes are inevitably characterized by limited control over the geometry. Investment casting with aluminium and steel has also been successfully applied to manufacture complex stochastic geometries, mostly for research purposes and for high relative densities. Today, the most effective manufacturing technology for accurate production of reticula of such complexity is additive manufacturing, especially through plastic/metallic powder-based techniques such as Selective Laser Sintering (SLS) or Binder Jetting (BJ) and photopolymers-based techniques such as Stereolithography (SLA) and Digital Light Processing (DLP). Useful materials may consequently be grouped in two families: polymers and metals; families with variegate mechanical properties not only between each other but also within the same family, alloy, and often production batch.

Nonetheless, for the present work it was fundamental to provide simple and predictive models without diving in detailed material analyses, for two reasons: first, that few parameters are commonly available in industry for standard purchases, especially for new or low performant plastics and alloys; second, that modelling base materials with accurate constitutive relations and failure implementations would exponentially increase the complexity of the models themselves, leading to model-dependent results and suffocating the global perspective.

Consequently, a simplified constitutive relation, a bi-linear elastic–plastic curve with zero slope plasticity trait, is considered sufficiently suited for the purpose: only two main parameters are needed, young modulus and yield stress. In terms of actual material properties, as said, materials analysed are ductile polymers and metals. As such the two aforementioned parameters are classified in six categories, considering a fixed stiffness (E) – commonly constant within the same polymer/alloy – and a variable yield (Y). In particular, the following ranges are considered:

1. low-performance polymers (LPP), $E = 1$ GPa, $Y = 10$–70 MPa, (polythene, polypropylene, ...);
2. engineering polymers (EP), $E = 2$ GPa, $Y = 30$–80 MPa (polyamide, polycarbonate, ABS, ...);
3. high-performance polymers (HPP), $E = 3$ GPa, $Y = 60$–120 MPa (PEEK, polyimide, ...);
4. aluminium alloys (AL), $E = 68$ GPa, $Y = 100$–500 MPa;

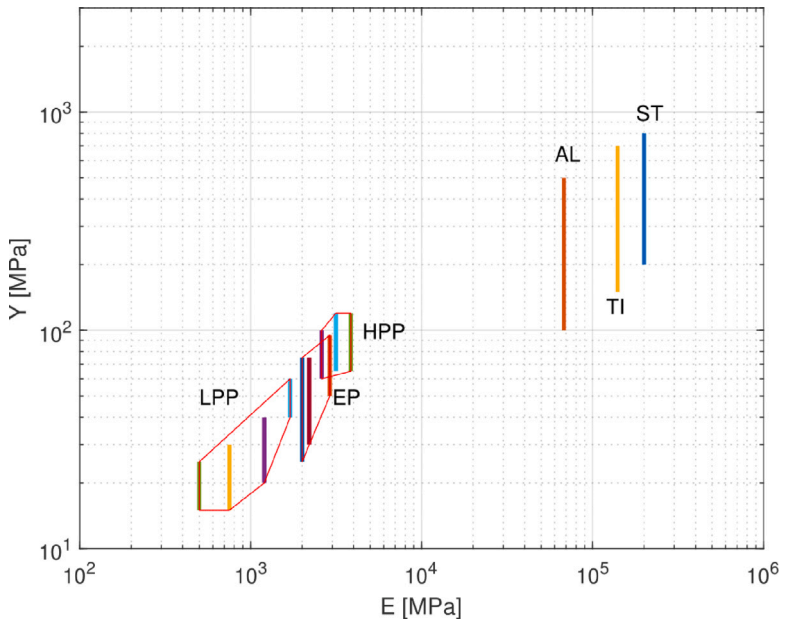

Fig. 10. Stiffness vs. yield for common metals and thermoplastics and chosen ranges. Logarithmic scale is used for improved clarity.

5. titanium alloys (TI), $E = 140$ GPa, $Y = 150$–600 MPa;
6. steel alloys (ST), $E = 200$ GPa, $Y = 200$–800 MPa.

Values are chosen in order not to overcome physical boundaries, in particular in terms of yield/stiffness relations. Fig. 10 shows such relations for the categories involved.

Base material densities were chosen accordingly to average literature values, for instance 2.7 and 7.8 g/cm^3 respectively for aluminium and steel alloys.

2.3.3. Model setup and analyses outputs

Cellular solids described at the beginning of the current section present, regardless of their base material but especially for elastic–plastic cases, a bi-linear compressive behaviour with zero-slope collapse stress. Such behaviour is completely defined by analogous parameters as for the material base: stiffness (E_{ret}) and collapse stress (Y_{ret}). Notable is the fact that part of the curve is sufficient to define the whole up to densification: assuming the behaviour reported at Fig. 1, compressive analyses need only to be carried out up to collapse, or immediately after. On the other hand, such approach prevents the appreciation of the densification phase, which commonly triggers at strain values of 50%–70% (Li et al., 2006); however, densification phase is a drastically different physical problem, where self-contacts and material failure are much more significant. Given the necessity to keep simple modelling strategies for the base materials and the purpose of providing simple output relations, the issue is here considered beyond the scope of the present work.

Neglecting contact and failure allowed to setup simulations with the implicit scheme, much faster for static analyses. The bottom of the reticula was constrained fixing the base nodes' translations, while the top nodes were imposed vertical translation at constant downward velocity and null translations for the two horizontal degrees of freedom (Fig. 11(a)). Analysis outputs are then calculated as depicted in Fig. 11(b): the reticulum stiffness (E_{ret}) is the tangent modulus, the collapse stress (Y_{ret}) is the maximum stress recorded. Example of a compressive analysis is shown in Fig. 12.

3. Results and discussion

The present section reports the parametric analyses, the results and the final discussion. Baseline are the findings collected by Gibson (2003), with the double purpose of validating the present models – and the entire procedure – with that robust literature and dive into the results to identify possible discrepancies.

Table 2
Density analyses – geometries.

Code	λ [mm]	D [mm]	α [–]	N [–]	avg. generations per subcase
L2D.8	2	.8	2.5	3, 4, 5	3
L3D.8	3	.8	3.75	5	3
L4D.8	4	.8	5	3, 5, 6, 7	3
L6D.8	6	.8	7.5	5	3
L8D.8	8	.8	10	3, 4, 5	3

First analysis is focused on density, producing fitted equations as a function of α. Then, boundary and stochasticity effects are systematically studied in compression and tension and optimal values of characteristic dimensions for subsequent analyses are found. The third and most important phase is then the parametric analysis: compression properties of reticula of various relative densities are reported, compared and related to the literature relations valid for classical open-cell foams. Last, validation is performed, with two different strategies for plastics and metals.

3.1. Density

The first parameter under analysis is the relative density. Purpose is to define a relation between the slenderness ratio α and the relative density RD of the reticulum. In order to obtain reliable results, paramount is the evaluation of cell sensitivity and boundary effects.

Consequently, a first analysis is performed on a selection of five notable values of α, obtained fixing D to 0.8 mm and variating λ, as reported in Table 2.

As seen in Fig. 13, the Voronoi reticulum has evident boundaries which are non-conformal to the Voronoi tessellation but come from the boolean cut; cut that produces a region where the struts are not contributing to the structural response, as averagely linked to only one of the sample points. In order to take the problem into account in the density evaluation, such boundary is estimated to be half of the characteristic length λ, and the models are cut consequently, evaluating their relative density before and after the cut.

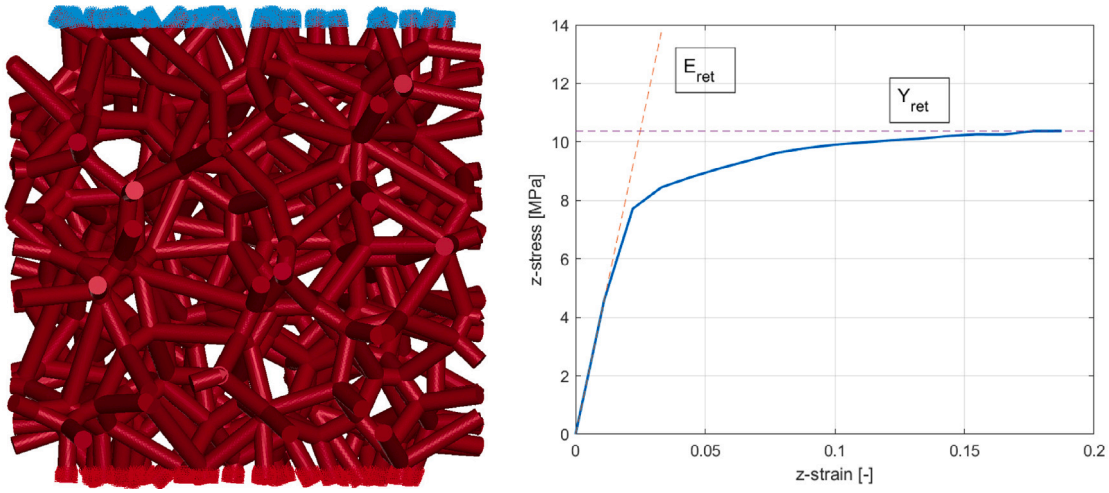

(a) Setup (b) Outputs

Fig. 11. Analysis setup and outputs.

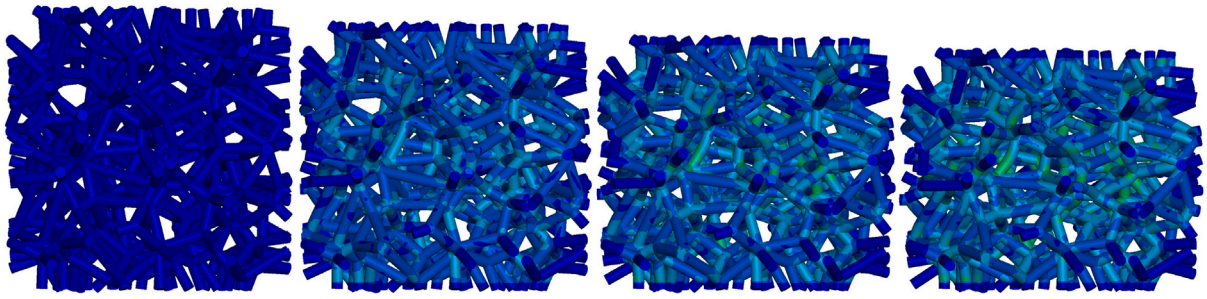

Fig. 12. Example of compressive analysis.

It is important to note that such treatment is inevitably extended to the calculation of any other global structural parameter: evaluation of both global strain and stress for a cubic reticulum involves the normalization of displacement (Δz) and force (F_z) with respectively initial length (L_z) and resisting area (A_0). Nonetheless, assuming that the whole structure is contributing to the structural behaviour could lead to misleading results, difficult to compare when different α are analysed. As such, all global parameters are calculated considering the cut *resisting cube*, as follows (Eqs. (8), (9)):

$$\varepsilon_{global} = \frac{\Delta z}{L_z} = \frac{\Delta z}{\lambda(N-1)} \tag{8}$$

$$\sigma_{global} = \frac{F_z}{A_0} = \frac{F_z}{\lambda^2(N-1)^2} \tag{9}$$

Subsequently, density is evaluated for increasing characteristic dimensions for all the subcases presented in Table 2. Measurement of both the whole structure as it is once exited from the loop at Fig. 6 and of the post-processed structure with adjusted boundaries are carried out.

For the sake of brevity, full results of only one subcase are here reported, in particular "L4D.8", $\alpha = 5$. Such results, reported in Fig. 14, show hyperbolic trends with asymptotic relative density for both measurement methods. Notable is the fact that the cut procedure is characterized by a negative slope trend, while the other by a positive slope; in other words, at low values of N performing a cutting of the boundaries as described above leads to overestimation of the density, while measuring the density on the whole cubes leads to considerable underestimation. Such peculiarity seems to suggest that an optimal cutting value for density measurement may be present and worth searching.

Analysing results in Fig. 14 from another perspective, it is clear that the stochasticity effect reaches acceptable values when $N = 5$, with maximum standard deviation measured at 0.3%. The present result is important as leads to a second analysis, a thorough evaluation of the density for multiple values of α at $N = 5$, assuming negligible randomness effects for that characteristic dimension. It was decided to proceed with the redundant double measurement methods and consequently take as finalized values the averages: the choice is intended to project the results to $N = \infty$.

Final density results, reported in Fig. 15, follow an exponential trend as a function of α, for which best fittings is reported below, Eq. (10):

$$RD(\alpha) = ae^{b\alpha} + ce^{d\alpha} = (.28 \pm .07)\, e^{(-.25 \pm .03)\alpha} + (2.19 \pm .7)\, e^{(1.01 \pm .19)\alpha} \tag{10}$$

Proposed fitting is compared to the fitted Gibson–Ashby relation (Gibson, 2003) (Eq. (1)): respectively, Eqs. (11) and (12). Values are reported with their uncertainties, 95% confidence bounds.

$$RD(1/\alpha) = a\left(\frac{t}{l}\right)^2 + b\left(\frac{t}{l}\right) + c = (1.35 \pm .15)\left(\frac{t}{l}\right)^2 + (.30 \pm .07)\left(\frac{t}{l}\right) + (-.02 \pm .005) \tag{11}$$

$$RD(1/\alpha) = C\left(\frac{t}{l}\right)^2 = C\left(\frac{1}{\alpha}\right)^2 = (2.08 \pm .07)\left(\frac{1}{\alpha}\right)^2 \tag{12}$$

Comparison with the work from Gibson and Ashby shows suitability of their equation for a first approximation, while more accurate reproduction seems to need additional linear and constant terms.

Results obtained from the density analysis allowed to exploit Eqs. (10) and (11) for all the subsequent density evaluations. Consequently, values of relative density reported later on in the document as well as the ones reported in Table 1 must be interpreted as *predicted* relative densities evaluated by means of such equations.

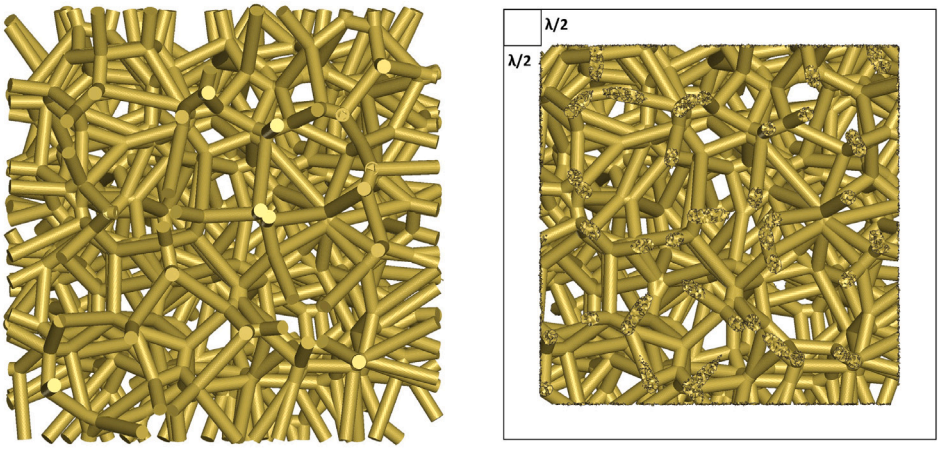

(a) Front view

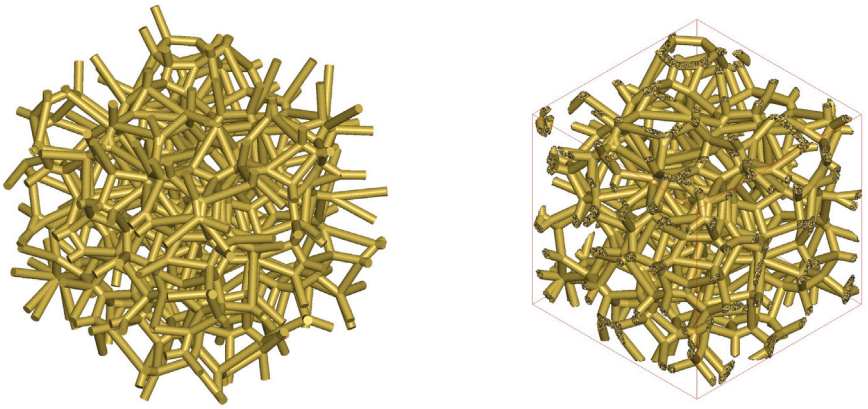

(b) Perspective view

Fig. 13. Boundary treatment: on the left the whole cube, on the right its resisting sub-volume.

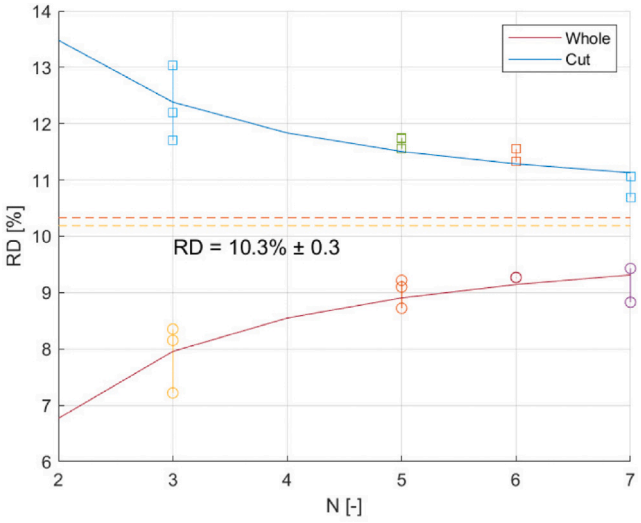

Fig. 14. Density evaluation on the whole and cut cubes, subcase "L4D.8".

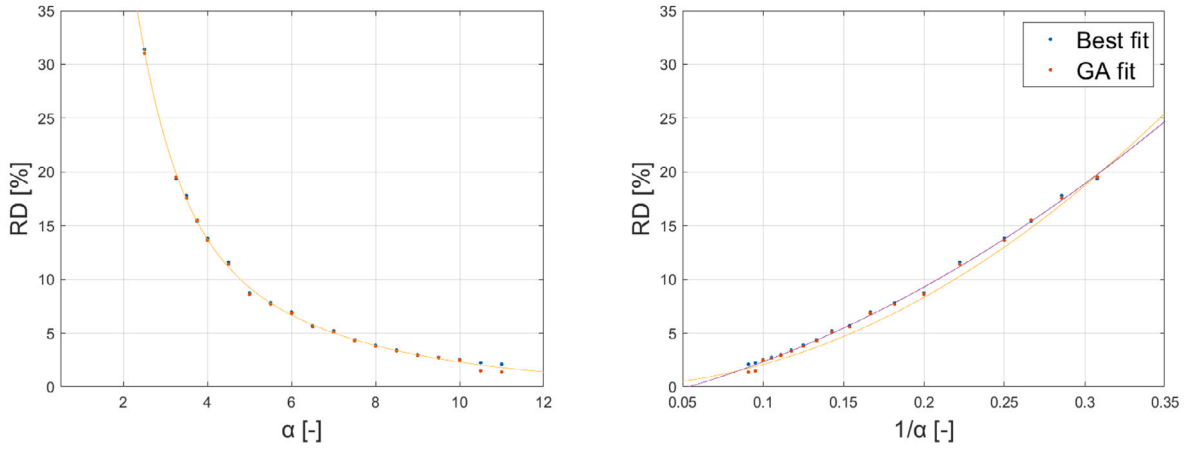

(a) RD vs α (b) RD vs $1/\alpha$

Fig. 15. Relative density as a function of α (a) and $1/\alpha$, proposed fitting vs. Gibson–Ashby equation.

Table 3
Sensitivity analyses – geometries.

Code	λ [mm]	D [mm]	α [–]	RD [%]	N [–]
L2D.8	3	.8	2.5	31.2	3, 4, 5
L4D.8	4	.8	5	9.3	3, 4, 5
L8D.8	8	.8	10	2.3	3, 4, 5

Table 4
Parametric analyses – geometries.

Code	λ [mm]	D [mm]	α [–]	RD [%]	N [–]
L3D.8	3	.8	3.75	15.4	5
L4D.8	4	.8	5	9.3	5
L6D.8	6	.8	7.5	4.3	5
L8D.8	8	.8	10	2.3	5

3.2. Sensitivity analyses

As an intermediate step to assure the reliability of the subsequent analysis, sensitivity study is performed to grasp the behaviour of the Voronoi reticula as a function of the number of the resisting cells and quantify the effect of the stochasticity on such behaviour.

To do so, three different combinations of the two main parameters are considered, each of them with three point cloud generations and three characteristic dimensions, for a total of 27 sample meshes (Table 3). Such models are then implemented in Ansys LS-DYNA and assigned simple material properties, typically traceable to a generic aluminium alloy; it is assumed that the material properties do not affect the sensitivity analysis results and as such the results reported below are valid to any base material. The material is implemented through a piecewise-linear plastic model: *MAT24 in LS-DYNA, chosen for its modelling simplicity, versatility and robustness. Material failure is set through a equivalent plastic strain threshold, fixed at 0.3; said failure implementation, arguably rather unphysical, is chosen to limit the structure behaviour to a failure point after which the curve is not considered: it is important to remind that the present analyses aim to study the sensitivity, and results have little physical meaning beside such aim.

Analysis performed are compression-tension implicit simulations, setup constraining two sets of nodes corresponding to $1/8^{th}$ of the cell characteristic dimension as described in paragraph 2.3.3. Results are shown in Figs. 16–18.

Results show two clear traits: first, that both the stochasticity and boundary effects fade away between $N = 4$ and $N = 5$. It is in fact evident that compressive and tensile analyses made with 5 cells give almost superimposable stress–strain curves, whilst 3-cells analyses show pronounced variability and sub-optimal behaviours, especially towards failure. To quantitatively describe the cell sensitivity and the uncertainty due to stochasticity, two main parameters are extracted: the first is the tangent modulus of the stress–strain curve, the second is the total work up to the last available strains prior to failure. Results are shown in Fig. 19.

It is here important to note that at $\alpha = 5$ the intrinsic randomatic nature of the Voronoi reticula causes uncertainties over the mechanical response which are below 2%, while at the two analysed boundaries of the topology ($\alpha = 2.5$, thick beams, and $\alpha = 10$, slender beams) uncertainties, even if converging after 4–5 cells, maintain relatively high values (4%–6%). Such peculiarity suggests that Voronoi reticula present, in terms of repeatability, optimal values around $\alpha = 5$, and as such highest isotropy around that combination of the geometrical parameters.

In the end, sensitivity analyses showed that for both randomness and boundary effects 5 cells are enough to filter out any of the two within a maximum uncertainty reported at 6%.

3.3. Parametric analysis

The parametric analysis is setup with the four combinations of D and λ reported in Table 4, each with $N = 5$. Given the results provided in the previous paragraph, only one sample generation for each of the four combination was studied, being at $N = 5$ stochasticity and boundary effects established as negligible. Materials described in paragraph 2.3.2 were implemented in LS-DYNA with *MAT24, a piecewise-linear plastic model, without failure in order not to slip into unphysical behaviour.

Analyses were performed via the LS-DYNA software LS-OPT, fixing the material stiffness E and variating the material yield Y. Output parameters are defined as E_{ret} and Y_{ret}, respectively stiffness and collapse stress of the reticulum. Results are plotted in Figs. 20 and 21, as material stiffness vs. stiffness ratio and material yield vs. yield ratio. It is here remarked that reticula stiffness and stress are both treated as described in paragraph 3.1, complying to the concept of the resisting cube.

Notable results are mainly three. First, relative density is not sufficient to describe the reticula behaviour, as the yield ratio is not constant for fixed relative density (Fig. 21). On the other hand, the reticulum stiffness confirms its dependency on the sole relative density, as little variation is shown as a function of the base material modulus, and only for high relative densities (Fig. 20). Last, a strong mismatch between the theoretical values calculated with the Gibson–Ashby relations at Eqs. (2) and (3) and the numerical results here described is evident.

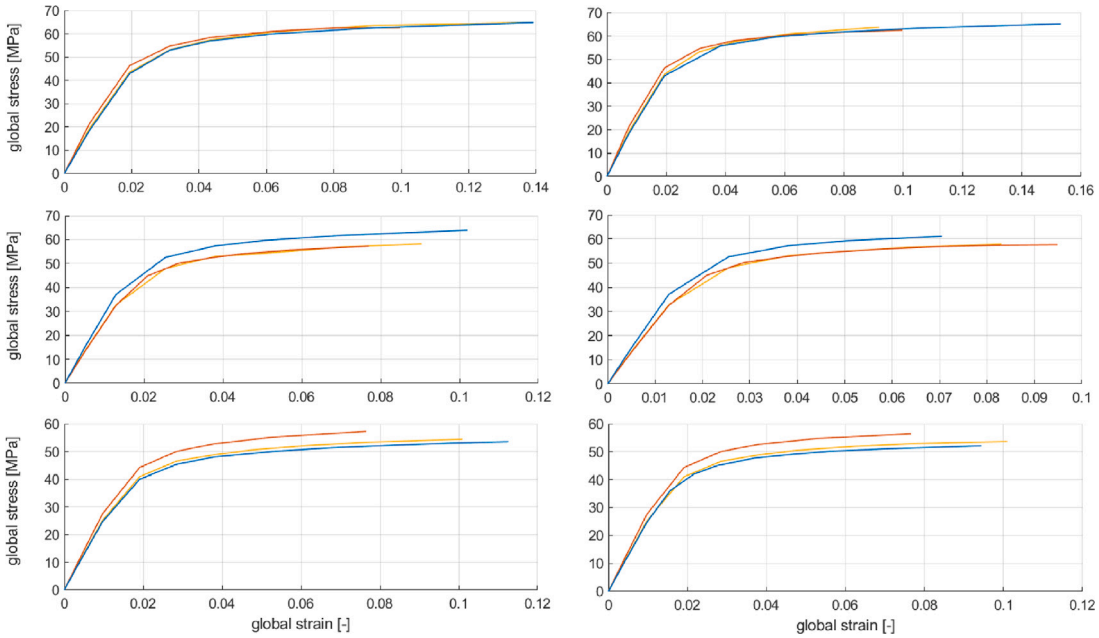

Fig. 16. Compression-tension (left–right) analyses for $\lambda = 2$, $D = 0.8$M; from the top: $N = 5, 4, 3$.

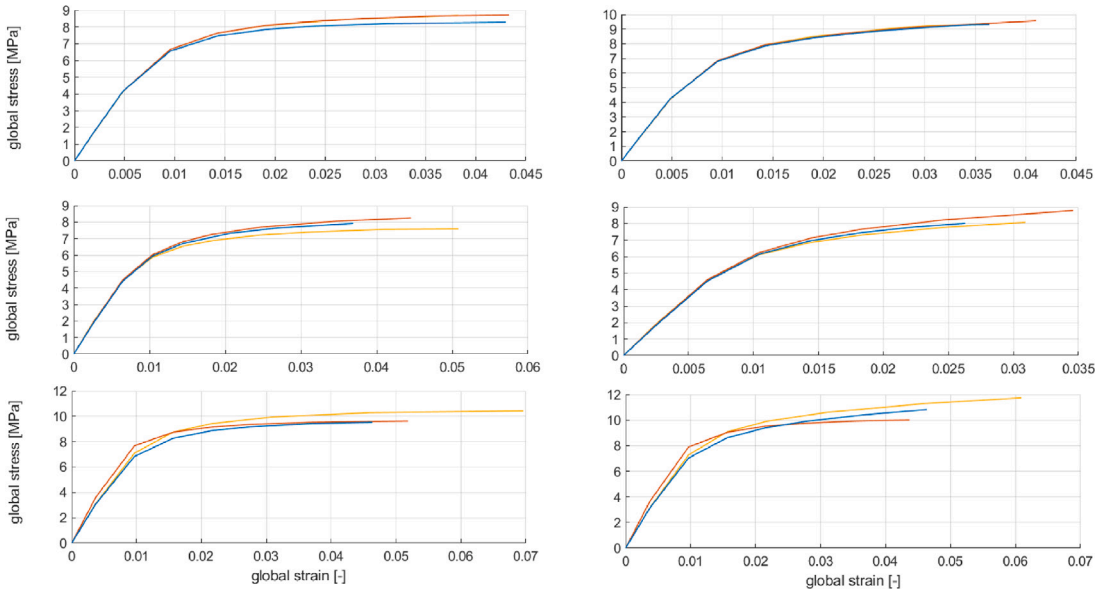

Fig. 17. Compression-tension (left–right) analyses for $\lambda = 4$, $D = 0.8$M; from the top: $N = 5, 4, 3$.

Both for stiffness and collapse stress, it is clear that said relations underestimate the reticula properties: in relative terms, the lower the reticulum relative density, the larger is such underestimation. In order to better appreciate this finding, results for a stainless steel alloy largely used in additive manufacturing (AISI 316L, $Y = 470$ MPa) are shown in Fig. 22. With respect to the results shown at the end of the density analysis (Section 3.1), Gibson–Ashby analytical equations need notable modifications to properly fit the numerical data, in particular for the collapse stress approximation. Best approximations, reported in Eqs. (13) and (14), are second order polynomials for both cases.

$$E(RD) = a\ RD^2 + b\ RD + c = (1.68 \pm 2.27)\ \ RD^2 + (-0.01 \pm 0.23)\ \ RD + (0.0 \pm 0.01) \tag{13}$$

$$Y(RD) = a\ RD^2 + b\ RD + c = (2.67 \pm 2.27)\ \ RD^2 + (0.10 \pm 0.41)\ \ RD + (0.0 \pm 0.01) \tag{14}$$

3.4. Validation

Given the complex manufacturability, experimental validation is inevitably performed in few points, with separate strategies for plastics and metals.

3.4.1. Plastics

Plastics' validation is carried out experimentally by producing and testing a series of Voronoi samples in nylon, through the SLS technique. Such specimens, of which specifics are reported in Table 5 and pictures are shown in Fig. 23, have been produced by the additive manufacturing company cirp GmbH with a nylon powder whose mechanical

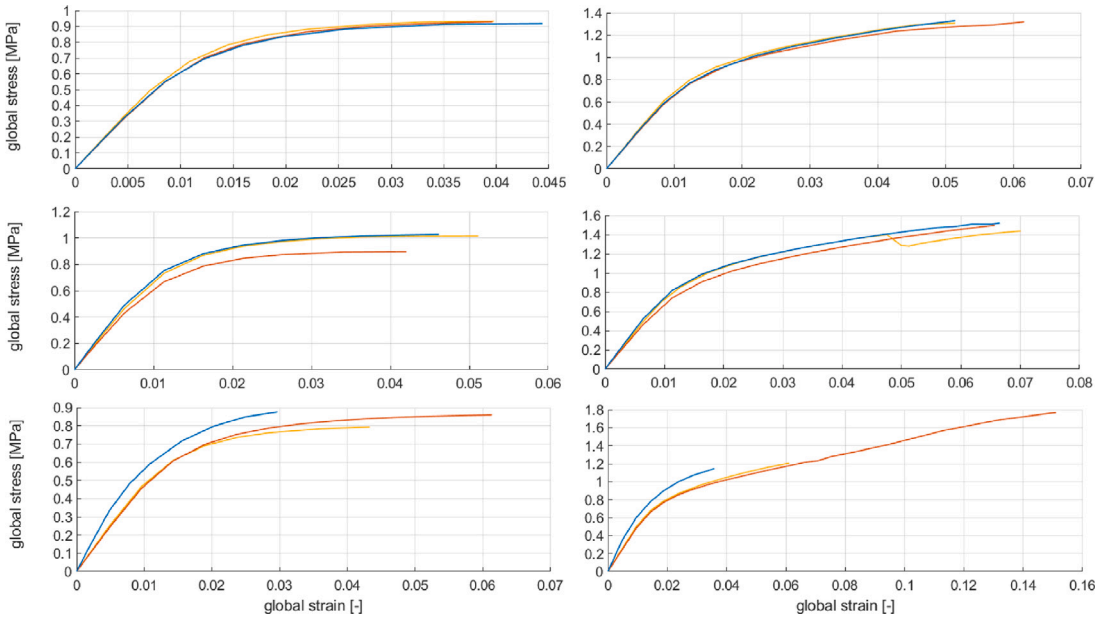

Fig. 18. Compression-tension (left–right) analyses for $\lambda = 8$, $D = 0.8$M; from the top: $N = 5, 4, 3$.

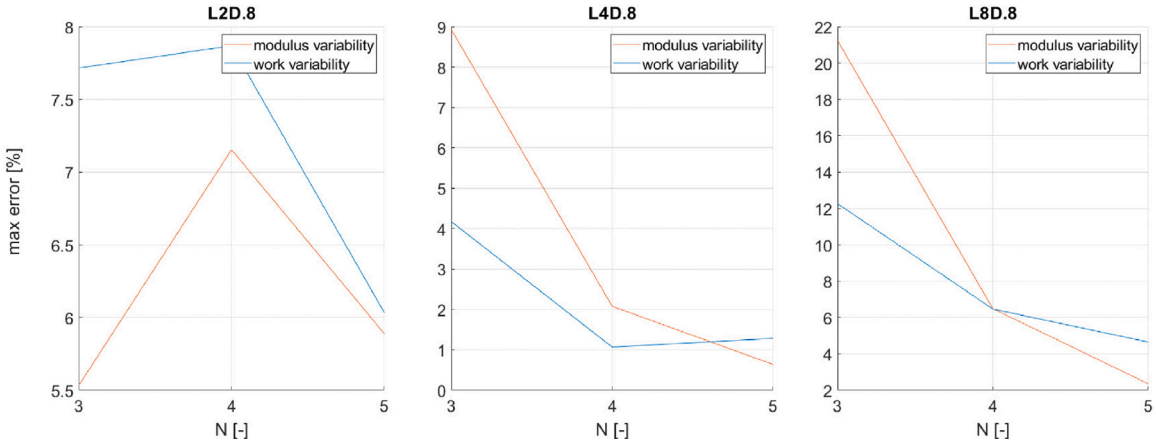

Fig. 19. Stochasticity effects as function of the number of cells.

Table 5
PA12 compression test – samples.

Samples	Dim. [mm × mm × mm]	$N_x \times N_y \times N_z$ [–]	λ [mm]	D [mm]	α [–]	RD [%]
1	35 × 35 × 25	9 × 9 × 6	4	0.8	5	9.3
2	35 × 35 × 25	7 × 7 × 5	5	0.8	6.25	6.2
3	35 × 35 × 25	6 × 6 × 4	6	0.8	7.5	4.3

properties, available in literature (Cobian et al., 2022), are the following (vertical loading direction): elastic modulus of 1.4 GPa and yield stress of 25.0 MPa.

Quasi-static compression tests were performed with an MTS 858 with speed set at 5 mm/min.

Reticulum properties are extracted from the graphs at Figs. 20 and 21: for specimens 1 and 3 direct information are available due to the numerical simulations performed at $\alpha = 5$ and $\alpha = 7.5$, while for specimen 2 the reticulum properties are linearly interpolated between the two.

Results, shown in Fig. 24, present good correlation especially in terms of collapse stress for all the three cases examined, with slight overestimation of specimen 2 due to the linear interpolation procedure. Such overestimation disappear when the quadratic nature of the solution is considered and a more appropriate interpolation is carried out accordingly. The elastic modulus is instead slightly overestimated for each of the three cases, likely due to the simplified nature of the material approximation, which actually present a non-linear elasticity. Overall, the experimental curves are well-captured in all the three cases analysed, especially in terms of total absorbed energy.

3.4.2. Metals

Validation for metals is problematic, primarily because accurate additive manufacturing of a stochastic Voronoi geometry is difficult to achieve with current technologies; foams on the other hand, even if available in many different forms, are not geometrically compliant with Voronoi geometries as explained in paragraph 2.1, and their use for validation would need a separate study to properly take the topological differences into account.

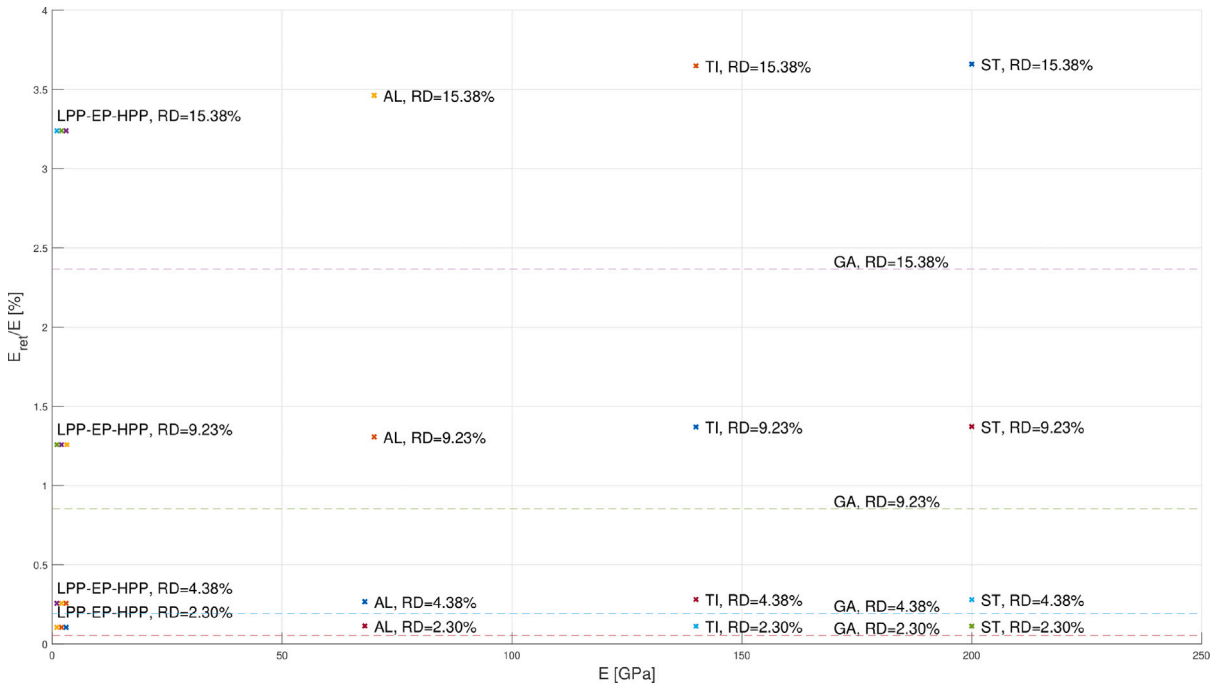

Fig. 20. Parametric analysis results – stiffness. Dashed lines represent the theoretical values as per Eq. (2), labelled points the numerical results for the materials analysed.

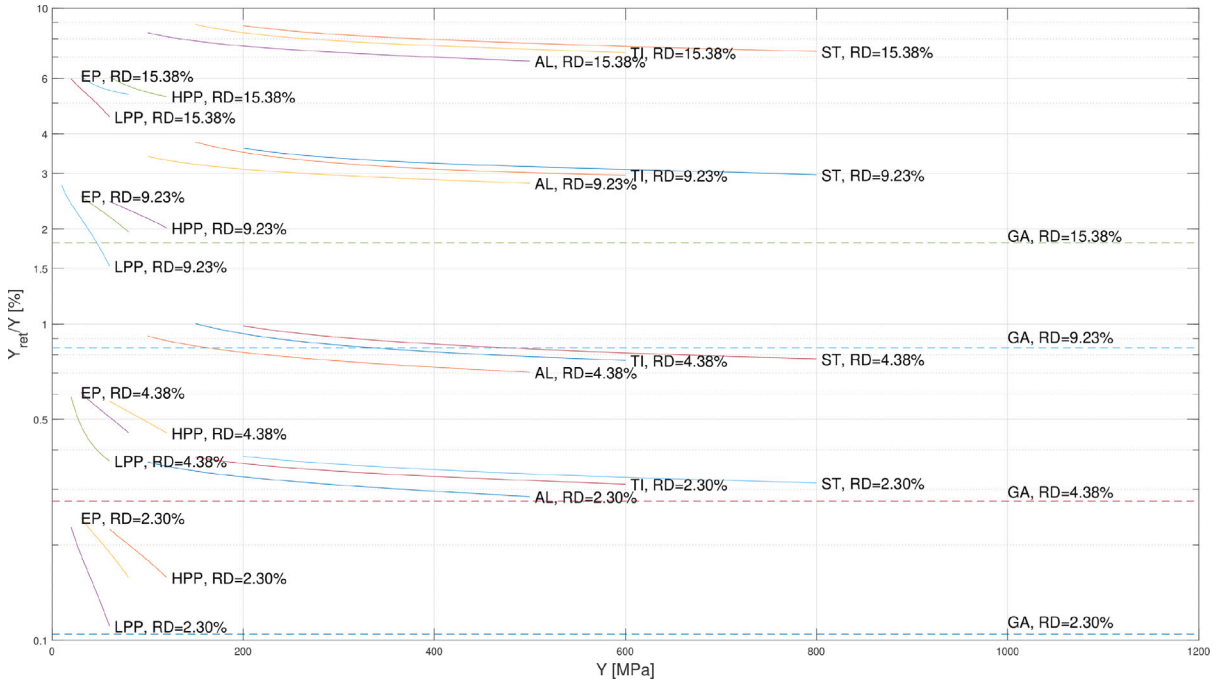

Fig. 21. Parametric analysis results – collapse stress. Dashed lines represent the theoretical values as per Eq. (3). A semi-logarithmic scale is used for best clarity.

Consequently, the task is approached in two stages: first, numerically by constructing an accurate model of a S275JR steel, for which comprehensive data and validated material implementations were internally available, second, by evaluating significant literature data, in particular Maliaris' studies (Maliaris et al., 2016).

For the numerical validation, again an elastic–plastic implementation of LS-DYNA *MAT24 was chosen, but in this case the full plastic curve was provided to the software for best description of the alloy plasticity. As for the main analyses at Section 3.3, implicit simulations were performed for best accuracy and only the first trait of the stress–strain curve is analysed, as sufficient to describe the foams' behaviour up to densification. Considered geometries are reported in Table 6. Even if the full stress–strain curve of a standard tensile test was available – and used to build the numerical model – a yield strength of $Y = 275$ MPa, minimum guaranteed for the considered alloy is used; the choice is related to the need to comply to an hypothetical evaluation based on the mechanical properties commonly available when similar alloys are purchased.

Results, shown in Fig. 25, are globally satisfactory, especially for the intermediate and low values of slenderness ratio and relative density (geometries 2,3,4). Sub-optimal correlation is however found for high

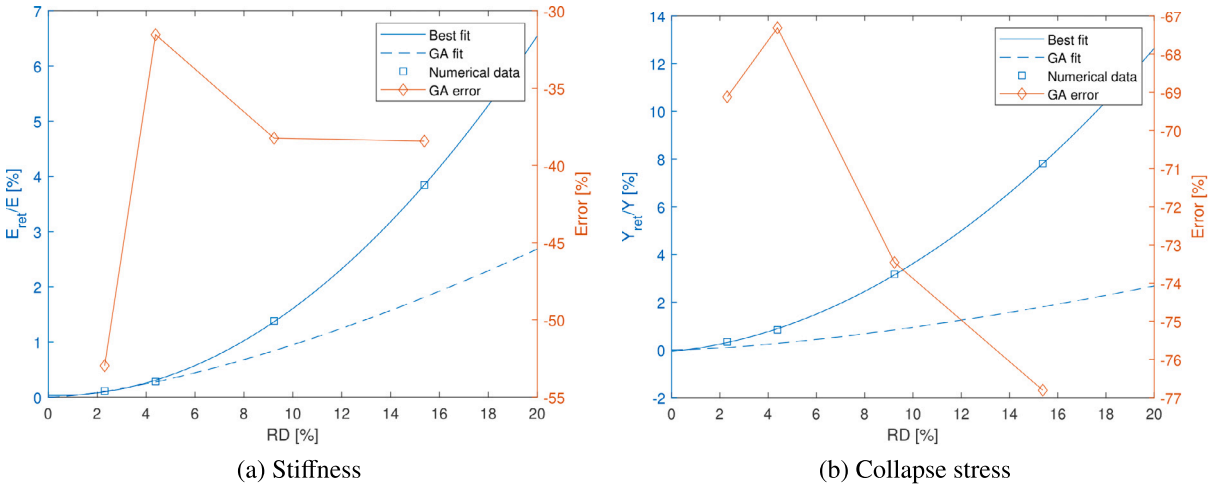

(a) Stiffness (b) Collapse stress

Fig. 22. Stiffness and yield ratio for AISI 316L ($Y = 470$ MPa), best Gibson–Ashby fit and results from parametric analysis.

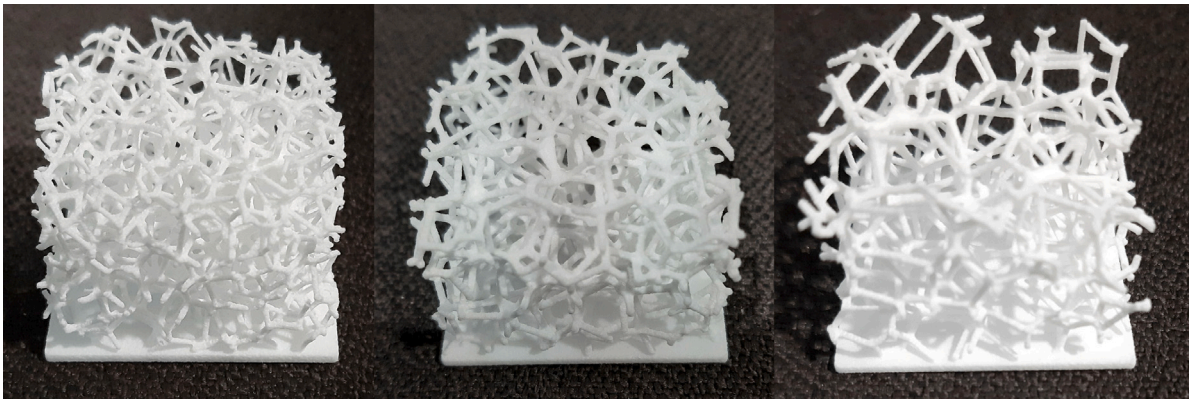

Fig. 23. PA12 compression test – samples 1,2,3 (left to right). The thin square plate visible at the bottom of each specimen was added for optimal centring and for maximization of friction with the base surface during compression.

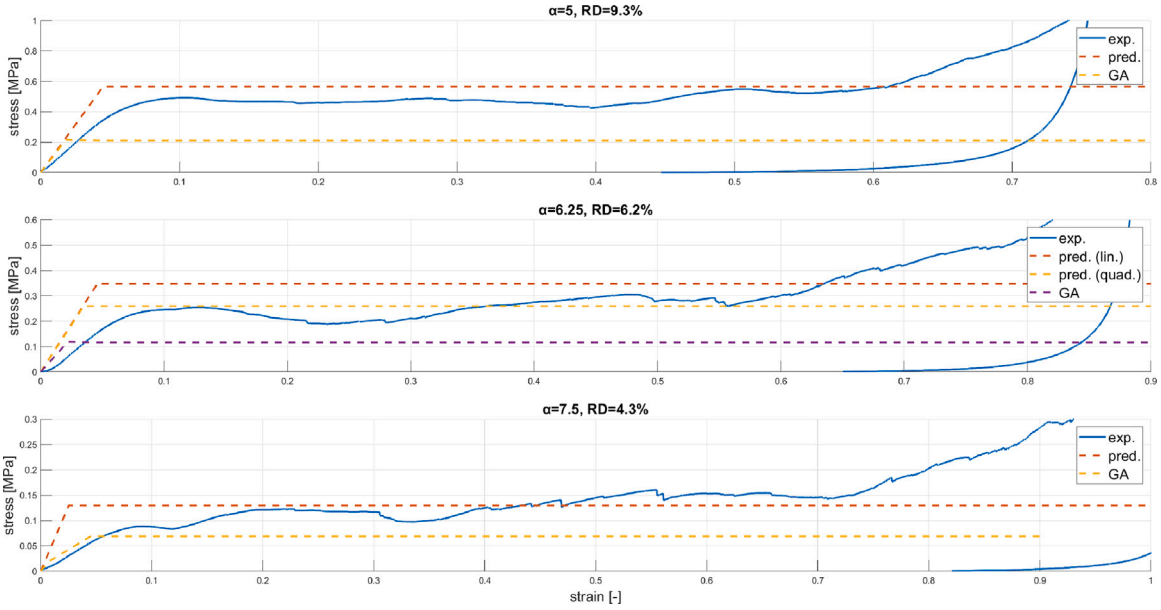

Fig. 24. Compression curves for PA12 specimens 1,2,3 (top to bottom), experimental results and predicted curves.

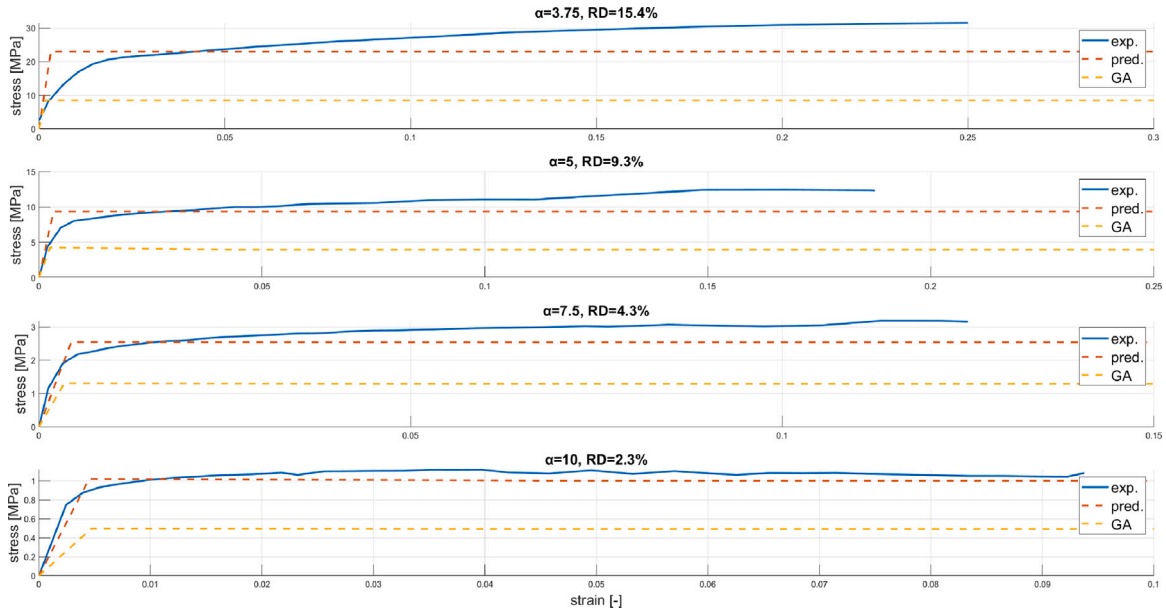

Fig. 25. Compression curves for S275JR specimens 1,2,3,4 (top to bottom), numerical results and predicted curves.

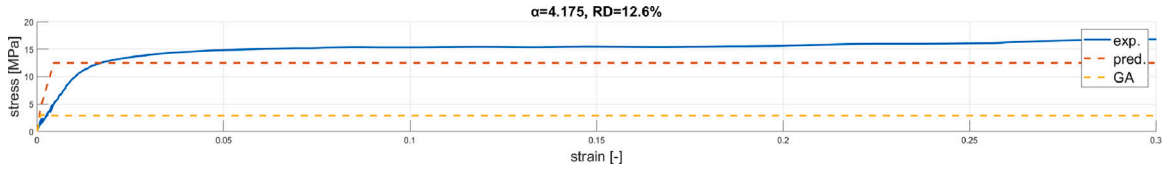

Fig. 26. Validation on Stainless Steel 304 lattice; α is estimated as explained in the text, while the curve is directly extracted and processed from Maliaris' work (Maliaris et al., 2016).

densities, with notable overestimation of the collapse stress and underestimation of the stiffness. As for the nylon specimens, such issues are likely consequence of the simple material approximation: in particular, as a linear elastic plastic law with zero-slope plasticity is considered hardening is not taken into account, thus explaining the difference increase towards densification. Being evident for geometry 1 only, it is clear that the problem becomes increasingly important as the geometry steps away from optimal values of density and structural efficiency, and the reticulum behaviour backs off in favour of an increasingly dominant material contribution.

The second stage is based on literature data. Amongst the studies cited in Section 1 directly focused on Voronoi lattices, most results are not suitable for a validation either for geometry/topology reasons, similarly to the open-cell foams, and for the high relative density of the analysed samples, outside the domain for the present analysis. However, the research published by Maliaris in 2016 (Maliaris et al., 2016) showed one notable case, the quasi-static compression of a lattice with $RD = 12.6\%$, produced with investment casting techniques in Stainless Steel 304. The density and strut diameter provided by the authors are used to extract the characteristic dimension $\lambda = 4.175$ mm through Eq. (10) and to estimate the slenderness ratio $\alpha = 4.175$. Finally, prediction of reticulum behaviour is carried out choosing average mechanical properties for the tested alloy, $Y = 215$ MPa; it is worth noting that the reticulum stress and strain are obtained in accordance to the concept of the resisting cube through Eqs. (8) and (9), in order to remain coherent with the constructed predictive model.

Analogously to the outcomes obtained for the numerical validation of the S275JR at high relative densities, results shown in Fig. 26 highlight slight underestimation of the reticulum collapse stress and overestimation of the stiffness. Again, such issues emerge at high relative density, where the simple material implementation show its limitations. Evident is, however, the large underestimation resulting from a classical approximation based on open-cell foams' equations.

Table 6
S275JR compression geometries.

Geometry	Dim. [mm × mm × mm]	N	λ [mm]	D [mm]	α [–]	RD [%]
1	15 × 15 × 15	5	3	0.8	3.75	15.4
2	20 × 20 × 30	5	4	0.8	5	9.3
3	30 × 30 × 30	5	6	0.8	7.5	4.3
4	40 × 40 × 40	5	8	0.8	10	2.3

3.5. Discussion

The results rose a few matters which are briefly discussed below.

First, the density of perfect three-dimensional reticula is globally well captured by literature analytical equations provided from experimental fittings of measurements performed on open-cell stochastic foams; as such, it is directly proportional to one parameter only, which is the thickness–length ratio t/l or the here defined slenderness ratio α. Best fittings are however identified in exponential equations as a function of α and second order polynomials as a function of $1/\alpha = t/l$.

The second paragraph 3.2 analysed the effects of the stochastic nature and of the boundaries of the Voronoi. First, it is found that for three-dimensional Voronoi a count of cells over each dimension equal or over 5 is sufficient to cancel out any boundary effect, with a stochastic contribution quantified at 6% at the extremes of the relative density domain, 2% at intermediate values. As N = 5 is later used for all the parametric analysis, these two values, summed to the uncertainty coming from the point generation method treated at paragraph

2.2.1, define the uncertainty for all the subsequent results: 11% at the boundaries of the domain, 7% at $\alpha = 5$.

The parametric analysis had a few notable outcomes. First, if stiffness and collapse stress are confirmed to be globally dependent on the relative density, with respect to Voronoi foams dependency is not unique, and both yield and stiffness present important contributions especially at high relative densities. Then, equations commonly used to fit stiffness and stress ratios as a function of the relative density resulted to be not suited for the analysed reticula; best fits are, for both cases, second order polynomials. Last, from the evaluation of the AISI 316L emerged that both collapse stress and stiffness are underestimated by the Gibson–Ashby equations, and as such underestimation present negligible variations as a function of the relative density, it is apparent an increase in the structural efficiency for highest slenderness ratios. The underestimation is likely caused by the imperfections present at the nodes in classical foams, where smooth fillets are commonly found and are main cause of an increase of relative density without parallel increase of structural properties.

Last, the whole analysis was validated with two different strategies for plastics and metals. The first were validated experimentally with SLS-produced nylon specimens; the second in two stages, numerically with further analyses on a validated model of a structural steel, experimentally through a notable literature case of quasi-static compression of casted stainless steel. Satisfactory results were achieved for both the material families as well as some clear limitations caused by the simple material implementation were reported, especially in terms of stiffness prediction and for high relative densities; in particular, it seems clear that the present analysis is valid for intermediate-to-low values of densities (< 10–15%), for which the structural behaviour can be assumed predominant with respect to the material's.

4. Conclusions

The work presented a systematic analysis of the static compressive properties of three-dimensional stochastic Voronoi reticula, with main purpose of constructing validated relations to be used within the additive manufacturing design loops, allowing prediction of the cellular properties for a generic base material. In detail, the work strived to relate simple base material parameters, modulus and yield stress, to the cellular behaviour, in terms of its stiffness and collapse stress. Base materials considered were ductile plastics and metals.

Voronoi reticula were built with a dedicated routine completely based on open-source and free software to allow repeatability, with a direct construction of both geometry files for manufacturing and high quality solid tetrahedral meshes. After proper analysis of boundary and randomness effects, parametric finite element analyses were performed, providing direct relations between input and output parameters. Validation was then performed experimentally and numerically, achieving satisfactory correlation with both strategies and confirming the suitability of the material approximation and validity of the chosen approach.

The analyses provided novel insights in the study of stochastic Voronoi reticula, exposing unsuitability of classical analytical equations historically used for prediction of the compressive behaviour of similar structures, the open-cell foams. Such equations, based solely on the relative density, showed a clear underestimation of the cellular mechanical properties, likely due to the geometrical imperfections present in natural foams.

However, this discrepancy has not been fully investigated here and needs proper attention in future works to be satisfactorily quantified: in particular, numerical models of filleted, imperfect reticula need to be constructed and their response evaluated and compared to ideal perfect reticula as a function of the fillets' topology, shape and dimensions. Focus must be put in obtaining proper understanding of the filleting effects on the reticulum properties and in developing correction strategies over density, stiffness, and collapse stress to translate the vast available knowledge on open-cell foams to geometrically perfect stochastic lattices.

Subsequently, developments of the work are gradual sophistication of material approximations to improve final correlation and introduce prediction of densification, study of strain rate dependency and impact absorption performances, investigation of other stochastic geometries and graded reticula.

Declaration of competing interest

The authors declare that they have no known competing financial interests or personal relationships that could have appeared to influence the work reported in this paper.

Data availability

The code lattice300 developed to generate the models is freely available on GitHub. Other data will be made available upon request.

Acknowledgements

This research was supported by the company cirp GmbH (https://www.cirp.de/verfahren/rapid-prototyping_EN.php5). In particular, fundamental support was provided in samples' manufacturing by Ubiratan S. Freitas, Fatma Karayagiz and Hans Nopper.

References

Al-Osman, O., Alkhader, M., Abuzaid, W., 2023. Enhancing the multifunctionality of open-cell foams through tailoring their thermal and mechanical properties using coatings. Eur. J. Mech. A Solids 99, 104923.

Andrews, E., Sanders, W., Gibson, L.J., 1999. Compressive and tensile behaviour of aluminum foams. Mater. Sci. Eng. A 270 (2), 113–124.

Arcaro, S., Maia, B.G.d.O., Souza, M.T., Cesconeto, F.R., Granados, L., Oliveira, A.P.N.d., 2016. Thermal insulating foams produced from glass waste and banana leaves. Mater. Res. 19, 1064–1069.

August, A., Nestler, B., 2020. About the surface area to volume relations of open cell foams. Eng. Res. Express 2 (1), 015021.

Azzi, W.E., et al., 2004. A systematic study on the mechanical and thermal properties of open cell metal foams for aerospace applications.

Barber, C.B., Dobkin, D.P., Huhdanpaa, H., 1996. The quickhull algorithm for convex hulls. ACM Trans. Math. Softw. 22 (4), 469–483.

Bisht, A., Patel, V.K., Gangil, B., 2019. Future of metal foam materials in automotive industry. Automot. Tribol. 51–63.

Bornengo, D., Scarpa, F., Remillat, C., 2005. Evaluation of hexagonal chiral structure for morphing airfoil concept. Proc. Inst. Mech. Eng. G 219 (3), 185–192.

Chan, R., Nakamura, M., 1969. Mechanical properties of plastic foams: the dependence of yield stress and modulus on the structural variables of closed-cell and open-cell foams. J. Cell. Plast. 5 (2), 112–118.

Chen, J., Zhang, P., Cheng, Y., Liu, J., 2020. On the crushing response of the functionally graded metallic foams based on 3D Voronoi model. Thin-Walled Struct. 157, 107085.

Cobian, L., Rueda-Ruiz, M., Fernandez-Blazquez, J., Martinez, V., Galvez, F., Karayagiz, F., Lück, T., Segurado, J., Monclus, M., 2022. Micromechanical characterization of the material response in a PA12-SLS fabricated lattice structure and its correlation with bulk behavior. Polym. Test. 110, 107556.

Cook, R.L., 1986. Stochastic sampling in computer graphics. ACM Trans. Graph. 5 (1), 51–72.

Crow, F.C., 1977. The aliasing problem in computer-generated shaded images. Commun. ACM 20 (11), 799–805.

Dannemann, K.A., Lankford, Jr., J., 2000. High strain rate compression of closed-cell aluminium foams. Mater. Sci. Eng. A 293 (1–2), 157–164.

Davies, G., Zhen, S., 1983. Metallic foams: their production, properties and applications. J. Mater. Sci. 18, 1899–1911.

De Giorgi, M., Carofalo, A., Dattoma, V., Nobile, R., Palano, F., 2010. Aluminium foams structural modelling. Comput. Struct. 88 (1–2), 25–35.

Fiedler, T., Solórzano, E., Garcia-Moreno, F., Öchsner, A., Belova, I., Murch, G., 2009. Computed tomography based finite element analysis of the thermal properties of cellular aluminium. Mater.wiss. Werkst.tech. 40 (3), 139–143.

Frey, P.J., George, P.-L., 2007. Mesh Generation: Application to Finite Elements. Iste.

Gaitanaros, S., Kyriakides, S., 2015. On the effect of relative density on the crushing and energy absorption of open-cell foams under impact. Int. J. Impact Eng. 82, 3–13. http://dx.doi.org/10.1016/j.ijimpeng.2015.03.011, Metallic Foams under Dynamic Loading. URL https://www.sciencedirect.com/science/article/pii/S0734743X15000536.

Ge, C., Zhai, W., 2018. Cellular thermoplastic polyurethane thin film: preparation, elasticity, and thermal insulation performance. Ind. Eng. Chem. Res. 57 (13), 4688–4696.
Geuzaine, C., Remacle, J.-F., 2003. Gmsh Reference Manual. Free Software Foundation Inc., USA.
Geuzaine, C., Remacle, J.-F., 2009. Gmsh: A 3-D finite element mesh generator with built-in pre-and post-processing facilities. Internat. J. Numer. Methods Engrg. 79 (11), 1309–1331.
Gibson, L.J., 2003. Cellular solids. Mrs Bull. 28 (4), 270–274.
Hales, T.C., 2001. The honeycomb conjecture. Discrete Comput. Geom. 25, 1–22.
Hohe, J., Hardenacke, V., Fascio, V., Girard, Y., Baumeister, J., Stöbener, K., Weise, J., Lehmhus, D., Pattofatto, S., Zeng, H., et al., 2012. Numerical and experimental design of graded cellular sandwich cores for multi-functional aerospace applications. Mater. Des. 39, 20–32.
Huber, A., Gibson, L., 1988. Anisotropy of foams. J. Mater. Sci. 23, 3031–3040.
Jang, W.-Y., Kyriakides, S., Kraynik, A.M., 2010. On the compressive strength of open-cell metal foams with Kelvin and random cell structures. Int. J. Solids Struct. 47 (21), 2872–2883.
Kirpluks, M., Godina, D., Švajdlenková, H., Šauša, O., Modniks, J., Simakovs, K., Andersons, J., 2023. Effect of crosslink density on thermal aging of bio-based rigid low-density closed-cell polyurethane foams. ACS Appl. Polym. Mater..
Kumar, V., Manogharan, G., Cormier, D.R., 2009. Design of periodic cellular structures for heat exchanger applications. In: 2009 International Solid Freeform Fabrication Symposium. University of Texas at Austin.
Lagae, A., Dutré, P., 2008. A comparison of methods for generating Poisson disk distributions. In: Computer Graphics Forum, Vol. 27. Wiley Online Library, pp. 114–129.
Lautensack, C., Sych, T., 2006. 3D image analysis of open foams using random tessellations. Image Anal. Stereol. 25 (2), 87–93.
Li, Q., Magkiriadis, I., Harrigan, J.J., 2006. Compressive strain at the onset of densification of cellular solids. J. Cell. Plast. 42 (5), 371–392.
Limmahakhun, S., Oloyede, A., Sitthiseripratip, K., Xiao, Y., Yan, C., 2017. 3D-printed cellular structures for bone biomimetic implants. Addit. Manuf. 15, 93–101.
Linul, E., Serban, D.A., Voiconi, T., Marsavina, L., Sadowski, T., 2014. Energy-absorption and efficiency diagrams of rigid PUR foams. In: Key Engineering Materials, Vol. 601. Trans Tech Publ, pp. 246–249.
Maliaris, G., Lazaridis, T., Sarafis, I.T., Kavafaki, S., 2018. Indirect determination of the mechanical properties of stochastic lattices. In: MATEC Web of Conferences, Vol. 188. EDP Sciences, p. 02009.
Maliaris, G., Sarafis, E., 2017. Mechanical behavior of 3D printed stochastic lattice structures. In: Materials Structure & Micromechanics of Fracture VIII. In: Solid State Phenomena, vol. 258, Trans Tech Publications Ltd, pp. 225–228. http://dx.doi.org/10.4028/www.scientific.net/SSP.258.225.
Maliaris, G., Sarafis, I., Lazaridis, T., Varoutoglou, A., Tsakataras, G., 2016. Random lattice structures. Modelling, manufacture and FEA of their mechanical response. In: IOP Conference Series: Materials Science and Engineering, Vol. 161. IOP Publishing, 012045.
Maskery, I., Hussey, A., Panesar, A., Aremu, A., Tuck, C., Ashcroft, I., Hague, R., 2017. An investigation into reinforced and functionally graded lattice structures. J. Cell. Plast. 53 (2), 151–165.
Mueller, J., Matlack, K.H., Shea, K., Daraio, C., 2019. Energy absorption properties of periodic and stochastic 3D lattice materials. Adv. Theory Simul. 2 (10), 1900081.
Nelson, S., 2021. 32 Weird and wonderful fungi pictures. URL https://www.thephotoargus.com/weird-and-wonderful-fungi-pictures/.
Nguyen, C.H.P., Kim, Y., Do, Q.T., Choi, Y., 2021. Implicit-based computer-aided design for additively manufactured functionally graded cellular structures. J. Comput. Des. Eng. 8 (3), 813–823.
Oftadeh, R., Perez-Viloria, M., Villa-Camacho, J.C., Vaziri, A., Nazarian, A., 2015. Biomechanics and mechanobiology of trabecular bone: a review. J. Biomech. Eng. 137 (1).
Okubo, S., Yamauchi, Y., Kitazono, K., 2023. Effects of random and controlled irregularity in strut lattice structure of PA12 on compression anisotropy. Addit. Manuf. 63, 103385. http://dx.doi.org/10.1016/j.addma.2022.103385, URL https://www.sciencedirect.com/science/article/pii/S2214860422007746.
Ouellet, S., Cronin, D., Worswick, M., 2006. Compressive response of polymeric foams under quasi-static, medium and high strain rate conditions. Polym. Test. 25 (6), 731–743.
Papka, S.D., Kyriakides, S., 1998. Experiments and full-scale numerical simulations of in-plane crushing of a honeycomb. Acta Mater. 46 (8), 2765–2776.
Patten, W., Sha, S., Mo, C., 1998. A vibrational model of open celled polyurethane foam automotive seat cushions. J. Sound Vib. 217 (1), 145–161.
Raghavendra, S., Molinari, A., Cao, A., Gao, C., Berto, F., Zappini, G., Benedetti, M., 2021. Quasi-static compression and compression–compression fatigue behavior of regular and irregular cellular biomaterials. Fatigue Fract. Eng. Mater. Struct. 44 (5), 1178–1194.
Rahman, O., Uddin, K.Z., Muthulingam, J., Youssef, G., Shen, C., Koohbor, B., 2022. Density-graded cellular solids: Mechanics, fabrication, and applications. Adv. Eng. Mater. 24 (1), 2100646.
Sabet, S., Buonomo, B., Sheremet, M.A., Manca, O., 2023. Numerical investigation of melting process for phase change material (PCM) embedded in metal foam structures with Kelvin cells at pore scale level. Int. J. Heat Mass Transfer 214, 124440.
Schladitz, K., Redenbach, C., Sych, T., Godehardt, M., 2012. Model based estimation of geometric characteristics of open foams. Methodol. Comput. Appl. Probab. 14, 1011–1032.
Shinde, M., Ramirez-Chavez, I.E., Anderson, D., Fait, J., Jarrett, M., Bhate, D., 2022. Towards an ideal energy absorber: Relating failure mechanisms and energy absorption metrics in additively manufactured AlSi10Mg cellular structures under quasistatic compression. J. Manuf. Mater. Process. 6 (6), http://dx.doi.org/10.3390/jmmp6060140, URL https://www.mdpi.com/2504-4494/6/6/140.
Si, H., TetGen, A., 2006. A Quality Tetrahedral Mesh Generator and Three-Dimensional Delaunay Triangulator, Vol. 81. Weierstrass Institute for Applied Analysis and Stochastic, Berlin, Germany.
Stiapis, C.S., Skouras, E.D., Burganos, V.N., 2019. Advanced laguerre tessellation for the reconstruction of ceramic foams and prediction of transport properties. Materials 12 (7), 1137.
Sullivan, R.M., Ghosn, L.J., Lerch, B.A., 2008. A general tetrakaidecahedron model for open-celled foams. Int. J. Solids Struct. 45 (6), 1754–1765.
Vesenjak, M., Ren, Z., Öchsner, A., 2008. Behaviour of cellular materials under impact loading. Mater.wiss. Werkst.tech. 39 (2), 125–132.
Virtanen, P., et al., 2020. SciPy 1.0: Fundamental algorithms for scientific computing in Python. Nature Methods 17, 261–272. http://dx.doi.org/10.1038/s41592-019-0686-2.
Wang, F., Jiang, H., Chen, Y., Li, X., 2021. Predicting thermal and mechanical performance of stochastic and architected foams. Int. J. Heat Mass Transfer 171, 121139.
Wang, X., Lu, T.J., 1999. Optimized acoustic properties of cellular solids. J. Acoust. Soc. Am. 106 (2), 756–765.
Wejrzanowski, T., Skibinski, J., Szumbarski, J., Kurzydlowski, K., 2013. Structure of foams modeled by Laguerre–Voronoi tessellations. Comput. Mater. Sci. 67, 216–221.
Wen, C., Yamada, Y., Shimojima, K., Chino, Y., Hosokawa, H., Mabuchi, M., 2002. Novel titanium foam for bone tissue engineering. J. Mater. Res. 17, 2633–2639.
Yu, C.-J., Banhart, J., 1997. Mechanical properties of metallic foams. In: Proceedings of Fraunhofer USA Metal Foam Symposium, Stanton, Delaware. pp. 7–8.
Zhang, J., Ashby, M., 1992. The out-of-plane properties of honeycombs. Int. J. Mech. Sci. 34 (6), 475–489.
Zhang, M., Shang, J., Guo, S., Hur, B., Yue, X., 2021. Numerical investigation of effective thermal conductivity of strut-based cellular structures designed by spatial voronoi tessellation. Materials 14 (1), http://dx.doi.org/10.3390/ma14010138, URL https://www.mdpi.com/1996-1944/14/1/138.

Ivan Colamartino Ph.D. Candidate in Mechanical Engineering at LaST, crash laboratory in Polytechnic of Milan, Italy. The Ph.D. project is centred on impact and penetration behaviour of lattice materials.

Marco Anghileri Full Professor of Aerospace Structures and Passive Safety at Dpt. of Aerospace Science and Technology, Polytechnic of Milan, Italy. Areas of interest: aerospace structures, crashworthiness, impact mechanics, passive safety.

Marco Boniardi Full Professor of Metallurgy and Failure Analysis at Dpt. of Mechanical Engineering, Polytechnic of Milan, Italy. Areas of interest: failure analysis, forensic engineering, fracture mechanics, metallurgy.